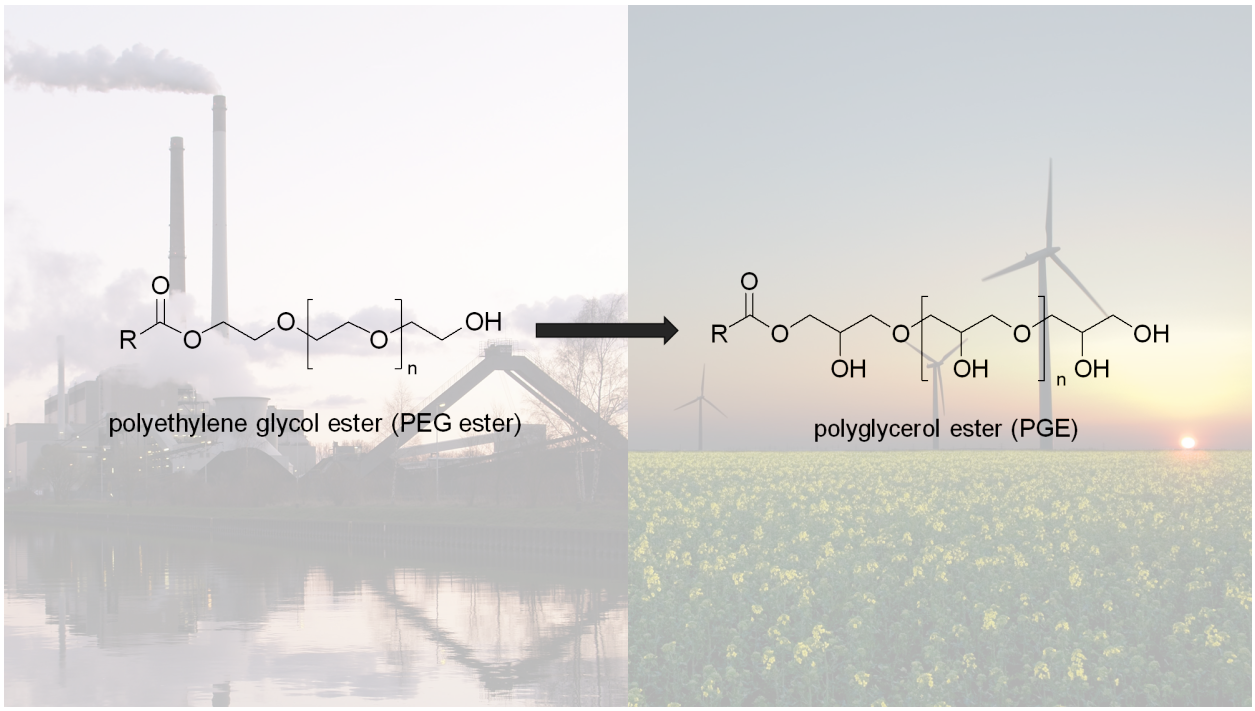

Synthesis and Characterization of Polyglycerol-based Surfactants

Master's thesis in Materials Chemistry

NIDHI BHAT

DEPARTMENT OF CHEMISTRY AND CHEMICAL ENGINEERING
CHALMERS UNIVERSITY OF TECHNOLOGY
Gothenburg, Sweden 2025
www.chalmers.se

Master's thesis 2025

Synthesis and Characterization of Polyglycerol-based Surfactants

NIDHI BHAT

CHALMERS
UNIVERSITY OF TECHNOLOGY

Department of Chemistry and Chemical Engineering
Division of Applied Chemistry
Chalmers University of Technology
Gothenburg, Sweden 2025

Synthesis and Characterization of Polyglycerol-based Surfactants
NIDHI BHAT

Supervisor: Romain Bordes, Applied Chemistry
Frida Bilén, Applied Chemistry
Examiner: Lars Evenäs, Applied Chemistry

Master's Thesis 2025
Department of Chemistry and Chemical Engineering
Division of Applied Chemistry
Chalmers University of Technology
SE-412 96 Gothenburg
Telephone +46 31 772 1000

Cover:
https://en.wikipedia.org/wiki/Emissions_trading
https://simple.wikipedia.org/wiki/Renewable_energy

Typeset in LaTeX
Printed by Chalmers Reproservice
Gothenburg, Sweden 2025

Synthesis and Characterization of Polyglycerol-based Surfactants
NIDHI BHAT
Department of Chemistry and Chemical Engineering
Chalmers University of Technology

Abstract

Polyglycerol-based surfactants have gained recognition as a renewable and safe alternative to polyethylene glycol-based surfactants, which are derived from fossil resources. Polyglycerol esters have a complex and polydisperse structure upon synthesis, which makes it difficult to pinpoint which characteristic of the compound is responsible for a certain property. It is therefore desirable to obtain monoesters as this would facilitate a more accurate comparison of the performance of different surfactants. To promote monoester formation, optimization of the synthesis was performed by fine-tuning the reaction conditions. The synthesized polyglycerol esters were characterized using various techniques. The results indicated that a higher molar ratio of polyglycerol to fatty acid promoted monoester formation. However, it is yet to be confirmed whether one-phase synthesis (in solvent) results in a higher monoester content than two-phase synthesis (solvent-free). The surfactants were also tested for their cleaning efficacy. A particular formulation of PG6C10 ester performed comparably to that of Berol O_X 91-6 (a polyethylene glycol-based surfactant), indicating that polyglycerol esters are a promising green alternative to fossil-based surfactants.

Keywords: Polyglycerol-based surfactant, polyglycerol ester, monoester, solvent synthesis, cleaning, renewable.

Acknowledgements

I would like to express my sincere gratitude to the Division of Applied Chemistry for providing a creative and supportive environment during my thesis work. I am especially thankful to my supervisors, Romain Bordes and Frida Bilén, and my examiner, Lars Evenäs, for their invaluable guidance and support throughout the course of my work. I would like to thank Hannes Schomaker, Eric Moilanen, Yiming Jia and Josmary Alejandra Velasquez Cano for their creative inputs and discussions that helped strengthen my research. Finally, I am grateful to my fellow master's students for making the work environment enjoyable and collaborative.

Nidhi Bhat, Gothenburg, June 2025

List of Acronyms

Below is the list of acronyms that have been used throughout this thesis listed in alphabetical order:

ATR	Attenuated Total Reflection
CMC	Critical Micelle Concentration
CPP	Critical Packing Parameter
DCM	Dichloromethane
DMF	N, N - Dimethylformamide
DMSO	Dimethyl Sulfoxide
EIC	Extracted Ion Chromatogram
ESI	Electrospray Ionization
FTIR	Fourier Transform Infrared
GLDA-Na_4	Tetrasodium Glutamate Diacetate
HLB	Hydrophilic-Lipophilic Balance
HPLC	High-Performance Liquid Chromatography
IFT	Interfacial Tension
IR	Infrared
IRE	Internal Reflection Element
KOH	Potassium Hydroxide
LC-MS	Liquid Chromatography-Mass Spectrometry
NaOH	Sodium Hydroxide
NMR	Nuclear Magnetic Resonance
PEG	Polyethylene Glycol
PGE	Polyglycerol Ester
PTSA	p-Toluenesulfonic Acid
ST	Surface Tension
SXS	Sodium Xylene Sulfonate

Nomenclature

Below is the nomenclature of the mathematical symbols that have been used throughout this thesis along with their units.

Mathematical symbols

γ	Interfacial tension ($\mathrm{mNm^{-1}}$)
$\Delta\rho$	Density difference ($\mathrm{kgm^{-3}}$)
g	Gravitational acceleration (9.8067 $\mathrm{ms^{-2}}$)
b	Radius of curvature at drop apex (m)
β	Bond number (dimensionless)
θ	Angle between interface tangent and horizontal (rad)
x	x coordinate (m)
y	y coordinate (m)
s	Arc length from drop apex (m)
X	x divided by b (dimensionless)
Y	y divided by b (dimensionless)
S	s divided by b (dimensionless)
D_e	Maximum diameter of drop (m)
D_s	Distance from the drop apex (m)
Γ	Surface excess concentration ($\mathrm{molm^{-2}}$)
Γ_∞	Maximum surface coverage ($\mathrm{molm^{-2}}$)
k_L	Langmuir constant ($\mathrm{Lmol^{-1}}$)
C	Concentration ($\mathrm{molL^{-1}}$)
R	Universal gas constant (8.314 $\mathrm{Jmol^{-1}K^{-1}}$)
T	Temperature (K)
σ	Surface tension ($\mathrm{mNm^{-1}}$)
A	Area per molecule ($\mathrm{Å^2}$)

N_A	Avagadro constant (mol^{-1})
θ_c	Contact angle ($^\circ$)

Contents

1
Introduction

1.1 Background

Surfactants are amphiphilic compounds that contain both hydrophilic and hydrophobic parts, and tend to position themselves at the interface between phases with varying levels of polarity, for example, gas-liquid and liquid-liquid interfaces [1]. Surfactants derived from non-renewable resources are produced in large quantities and used extensively. However, using these resources is not sustainable. As a result, there is a growing demand for eco-friendly alternatives to these surfactants.

Polyglycerol esters (PGEs) are non-ionic surfactants that serve as emulsifiers, wetting agents, and viscosity modifiers in the cosmetic, pharmaceutical, and food industries. They consist of a lipophilic moiety, which is a hydrophobic tail, and a hydrophilic moiety, which is a polyglycerol head. PGEs are considered a safer alternative to polyethylene glycol-based non-ionic surfactants, which are derived from fossil materials [2]. They also contain an ester bond, which facilitates biodegradability. Upon synthesis of PGEs, the surfactant structure obtained is usually complex. By fine-tuning the reaction conditions during synthesis, it may be possible to obtain a product with greater monodispersity, which is desirable so that the surfactants can be characterized in a better way.

However, the properties of PGEs are not yet completely understood. Hence, it is crucial to investigate them in more detail to facilitate a smooth transition to green surfactants.

1.2 Aim of the study

The aim of this thesis work is to better understand the properties of PGEs through their synthesis and characterization. Polydispersity makes it difficult to ascertain the properties of a surfactant, making it hard to pinpoint which characteristic of the compound gives rise to a particular property. It is therefore desirable to obtain a greater fraction of monoesters. A linear structure would allow for a more accurate comparison of the performance of different surfactants. To achieve this, fine-tuning of reaction conditions is necessary. This can be done, for example, by changing the ratio of the reactants, changing the catalyst used, or by changing the temperature and pressure at which the reaction takes place. Different research areas within the

domain of polyglycerol-based surfactants could then be evaluated, such as: (i) the effect of monoester content on the surface properties of PGEs, (ii) solubility and clouding phenomena of PGEs, (iii) the effect of surfactant composition in cleaning applications.

1.3 Limitations of the study

The following are the limitations of this thesis work: (i) the study is limited to polyglycerol esters, (ii) monoglycerides are not investigated, (iii) the chain lengths of the hydrophobic tails used are 10, 12 and 14 carbon atoms, and (iv) polyglycerol polyricinoleates and fatty acid chain polymerization are not investigated.

2
Theory

In this section, the theoretical framework, surfactant synthesis, characterization techniques employed in the project, and cleaning applications are described.

2.1 Polyglycerol-based Surfactants

Surfactants are amphiphilic molecules that are characterized by having hydrophilic and hydrophobic segments. They tend to partition at the interfaces between phases with differing polarities, for example, oil/water and air/water interfaces. This property enables them to engage in selective, preferential interactions at interfaces, leveraging their dual hydrophilic and hydrophobic nature. Typically, the hydrophobic segment consists of a hydrocarbon chain, while the hydrophilic head group can be ionic (either cationic or anionic), non-ionic, or amphoteric [1].

Polyethylene glycol (PEG)-based surfactants are the most commonly used non-ionic surfactants. However, a significant issue with these surfactants is the formation of 1,4-dioxane during ethoxylation, a toxic and harmful byproduct that makes it unsafe for human health. They are also derived from non-renewable resources, which make them disadvantageous. PGEs offer a potential alternative to PEG-based surfactants [2]. PGEs are non-ionic surfactants comprised of glycerol polymers esterified with fatty acids or interesterified with triglycerides. They are biodegradable, bio-compatible, non-toxic and non-carcinogenic, with no harmful effects observed even at a test concentration of 5 wt%. PGEs meet the criteria for safety, a bio-based economy, and sustainable development. Their applications are diverse, including use in the food industry, cosmetics, the pharmaceutical industry, etc [3].

2.2 Synthesis of Polyglycerol Esters

The synthesis of PGEs occurs through esterification, where polyglycerol reacts with fatty acid. The esterification of polyglycerols results in mixtures containing a wide variety of compounds due to the abundance of hydroxyl groups and the inherent complexity of commercially available polyglycerol mixtures. The hydrophilic–lipophilic properties of these esters, quantified using the Hydrophilic-Lipophilic Balance (HLB) concept, depend on factors such as the molecular weight of the esterified fatty acid, the degree of hydroxyl group esterified, and the number of glycerol units forming the polyglycerol backbone. A

decrease in the molecular weight of the fatty acid increases the hydrophilic nature of the ester, reflected by a higher HLB value. Conversely, an increase in the number of fatty acid moieties reacting with the polyol molecule results in a more lipophilic product, lowering the HLB value. For a specific fatty acid and degree of esterification, the hydrophilic nature increases with the molecular weight of the polyglycerol, due to a higher hydroxyl-to-fatty-acid ratio. Consequently, the complex mixtures of polyglycerol esters currently produced exhibit a broad HLB distribution.

In the commercial production of partial esters, the fatty acid moieties distribute across all available hydroxyl groups, with proportions primarily governed by thermodynamic factors, such as temperature and the molar ratio of reagents. As a result, the HLB value of the final product is lower than that of the pure monoester. To achieve HLB values closer to those of monoesters, a significant excess of polyglycerol is required during the reaction [4].

2.2.1 Synthesis

2.2.1.1 Solvent-free synthesis

PGEs can be synthesized through a reaction between a polyglycerol and a fatty acid with the help of a catalyst. It is a solvent-free two-phase synthesis performed at a high temperature and a low pressure to drive the reaction towards completion. The general reaction scheme employed in this work for the solvent-free synthesis of PGEs is illustrated in Figure 2.1. An excess of polyglycerol is often used to promote the formation of monoesters.

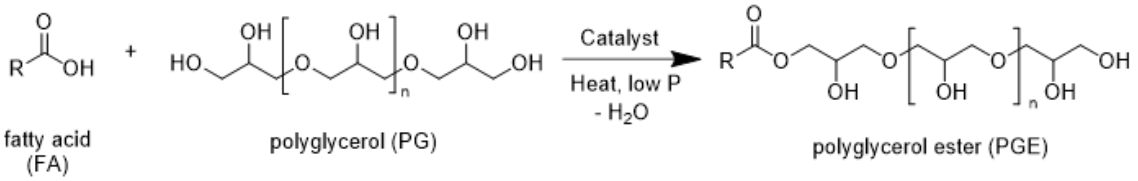

Figure 2.1: General reaction scheme for the solvent-free synthesis of PGEs, where R represents a linear hydrocarbon tail.

2.2.1.2 Synthesis in solvent

PGEs can be synthesized in solvent through a reaction between a polyglycerol and an activated acid in the form of an acyl chloride in the presence of a base, which neutralizes the formed hydrochloric acid and drives the reaction to completion. It is a one-phase synthesis performed at room temperature. The general reaction scheme employed in this work for the solvent synthesis of PGEs is illustrated in Figure 2.2.

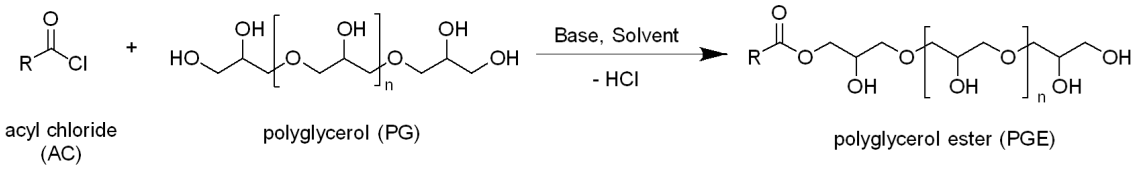

Figure 2.2: General reaction scheme for the solvent synthesis of PGEs, where R represents a linear hydrocarbon tail.

The hypothesis here is that synthesis in a one-phase system could promote monoester formation by managing the order of addition. If a solvent-free synthesis (a two-phase system) is considered, where the polyglycerol and the fatty acid are immiscible and present in a 1:1 molar ratio, it is possible that the esters that form at the interface remain there due to their surface activity. If this occurs, the fatty acid could continue to react with the polyglycerol head groups of the esters already at the interface, resulting in some unreacted polyglycerol. This would in turn result in the formation of diesters and triesters. If the synthesis occurs in a solvent where both the polyglycerol and the tail group are soluble, there is no such interface and the fatty acid would more likely react with a new polyglycerol molecule, forming a monoester. In such a case, excess polyglycerol would not be required to form monoesters. However, this hypothesis has not been confirmed.

2.3 Characterization of the surfactants

2.3.1 Chemical analysis

2.3.1.1 Liquid Chromatography-Mass Spectrometry

Liquid Chromatography-Mass Spectrometry (LC-MS) is an analytical technique that combines high-resolution chromatographic separation with sensitive and specific mass spectrometric detection. A typical LC-MS system integrates High-Performance Liquid Chromatography (HPLC) with mass spectrometry via an ionization source (interface). In this process, the sample is first separated by LC, and the resulting species are sprayed into an low pressure ion source, where they are converted into gas-phase ions. The mass analyzer then sorts these ions based on their mass-to-charge ratio, while the detector counts the ions emerging from the analyzer and may amplify the resulting signal. This process generates a mass spectrum, which is a plot of ion signals as a function of their mass-to-charge ratio. The mass spectrum is used to determine the elemental or isotopic composition of a sample, identify the masses of particles and molecules, and elucidate molecular structures [5].

2.3.1.2 Infrared spectroscopy

Infrared (IR) spectroscopy, particularly Attenuated Total Reflection (ATR) Fourier Transform Infrared (FTIR) spectroscopy, is another characterization technique used to elucidate the structures of the synthesized surfactants. ATR FTIR spectroscopy

works by directing infrared light at the interface between an infrared-transparent material with a high refractive index, known as the internal reflection element (IRE) (such as zirconium or diamond), and the sample positioned on the IRE surface [6].

2.3.1.3 Nuclear Magnetic Resonance spectroscopy

Nuclear Magnetic Resonance (NMR) is a highly effective technique for elucidating molecular structures, and interactions of surfactant-based compounds. It has distinct advantages over other methods, as it can directly offer insights into microscopic structures and interactions at the molecular level [7].

2.3.2 Physicochemical properties

2.3.3 Pendant drop tensiometry

Interfacial tension (IFT) and surface tension (ST) are key parameters commonly used to characterize an interface [8]. The driving force for surfactants to adsorb at an interface is to reduce the free energy of the phase boundary. The interfacial free energy per unit area indicates the work required to expand the interface. The term IFT is commonly used to refer to interfacial free energy per unit area. Therefore, the ST of a liquid is equivalent to the interfacial free energy per unit area at the boundary between the liquid and the air above it. When surfactant molecules cover this boundary, the ST (or the work needed to expand the interface) decreases. The more densely the surfactant molecules are packed at the interface, the greater the reduction in ST [9].

ST in liquids enables the formation of drops and is linked to the attractive forces between molecules. These forces arise from various interactions, including dispersion, dipole-dipole, dipole-induced dipole forces, and hydrogen bonding. In the bulk liquid, a molecule experiences equal attractive forces in all directions, but at the surface, this attraction is absent in one direction. This imbalance gives rise to surface energy, which is manifested in ST. Therefore, ST is a reflection of the cohesive forces within a liquid [10].

Pendant-drop tensiometry is based on the balance between gravity and the surface forces acting on a pendant drop, resulting in a distinctive drop profile. By analyzing this profile, the ST or IFT can be calculated using equation 2.1:

$$\gamma = \Delta\rho g b^2/\beta \tag{2.1}$$

Here, γ represents the IFT, $\Delta\rho$ is the density difference between the two phases, g denotes the gravitational acceleration, b is the radius of curvature at the drop's apex, and β is the Bond number, defined as $\beta \equiv \Delta\rho g b^2/\gamma$. The Bond number quantifies the relative significance of gravitational forces compared to interfacial forces.

The Bashforth and Adams equations, derived from the Laplace equation, define the drop profile as follows:

$$d\theta/dS = 2 - \beta Y - sin\theta/X \tag{2.2}$$

$$dX/dS = cos\theta \tag{2.3}$$

$$dY/dS = sin\theta \tag{2.4}$$

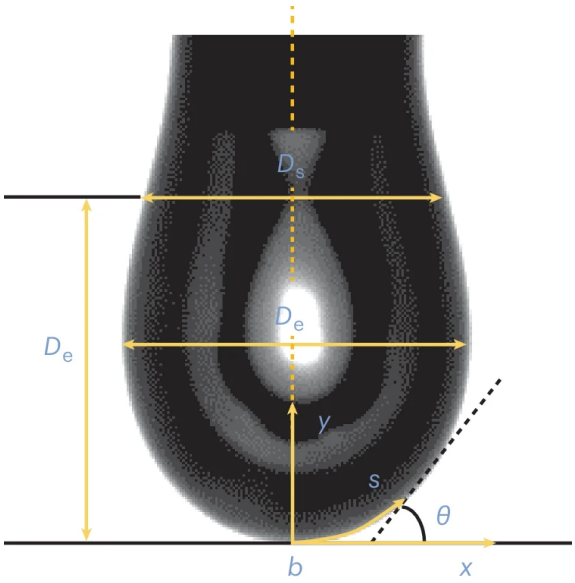

Figure 2.3: Schematic diagram of a pendant drop with the variables mentioned in this subsection [11].

Here, θ the angle between the interface tangent and the horizontal. If x and y are the coordinates, and s is the arc length from the drop apex, then X, Y, and S are dimensionless parameters obtained by dividing x, y, and s by the radius of curvature at the drop apex, b, respectively. By generating numerous theoretical dimensionless profiles, correlations between β and b can be established using measurable parameters, such as the maximum diameter D_e and the diameter at a distance D_s from the drop apex. A schematic diagram is shown in Figure 2.3 [11].

2.3.3.1 Critical Micelle Concentration

Surfactants are capable of self-assembly in solution. The concentration at which self-assembly begins is relatively well-defined and becomes even more precise with longer alkyl chains in the surfactant. The initial aggregates formed are typically nearly spherical in shape and are referred to as micelles. The concentration at which micelle formation starts is known as the critical micelle concentration (CMC). In water, aggregation occurs due to the insolubility of the non-polar

portions of the surfactant. The hydrocarbon chains pack together to minimize contact with water, while the hydrophilic interactions between the polar head groups create a repulsive force on the micelle surface. The head groups arrange themselves in a way that reduces these unfavorable repulsions [12].

Pendant drop tensiometry measurements result in an adsorption isotherm such as the one shown in Figure 2.4. The ST is constant at very low concentrations and then begins to decrease. Above a certain surfactant concentration, the ST becomes constant. This concentration is the CMC. The ST is constant because the unimer activity is constant above the CMC. Also, the slope of the curve just below the CMC is constant, suggesting that the adsorption is constant [10].

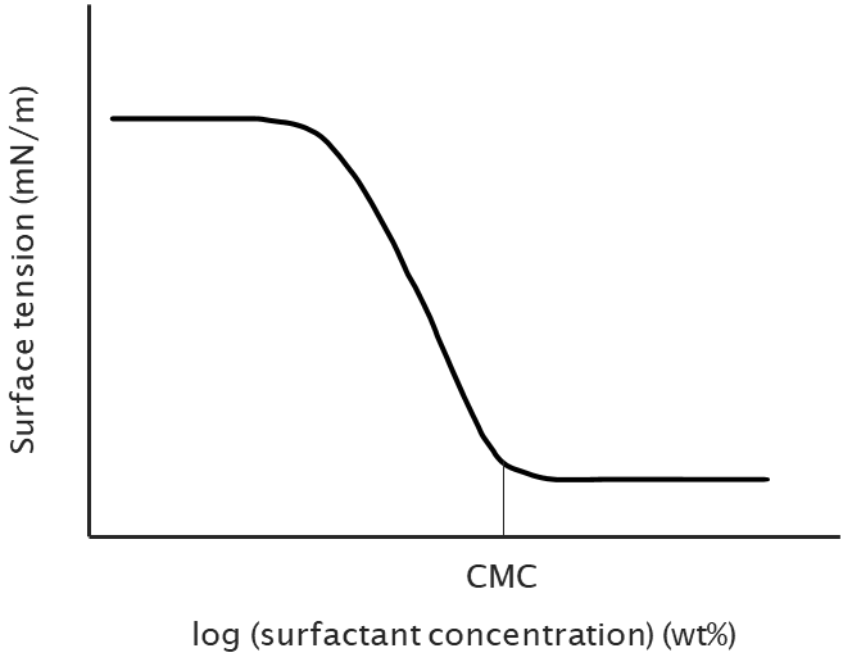

Figure 2.4: Typical adsorption isotherm obtained from pendant drop tensiometry measurements.

2.3.3.2 Gibbs adsorption isotherm

Gibbs adsorption isotherm takes the form of Equation 2.5 for non-ionic surfactants:

$$\Gamma = \frac{-1}{RT}\frac{d\sigma}{dlnC} \tag{2.5}$$

where Γ is the surface excess concentration, R is the universal gas constant, T is the temperature, σ is the surface tension and C is the surfactant concentration.

Equation 2.6 gives the surface excess concentration as a function of surfactant concentration from the ST data obtained from pendant drop tensiometry experiments. The slope of the curve of σ versus lnC can be used to calculate the surface excess concentration. This model is only applicable to concentrations below the CMC [13].

$$A = \frac{10^{23}}{N_A * \Gamma} \tag{2.6}$$

Equation 2.6 allows the calculation of the area per molecule A (Å^2) as a function of the surface excess concentration Γ (10^{-3} mol/m^2). N_A is the Avagadro constant.

2.3.3.3 Langmuir adsorption isotherm

Analyzing surfactant adsorption using a theoretical model is often useful to gain a molecular understanding. The parameters derived from this analysis can help explain the adsorption behavior of various surfactants and also predict adsorption in new systems [14].

The Langmuir isotherm is the simplest model that effectively describes the overall equilibrium behavior of a broad range of surfactants [15]. The Langmuir equation is derived based on the assumptions that (i) the surface is homogeneous, (ii) the surfactant adsorbs in a single layer, (iii) there are no interactions between a surfactant and water or between two surfactants, and (iv) the surfactant and water molecules are of equal size, thus having identical cross-sectional surface areas. The first two assumptions are reasonable, but the last two are not. Research has shown that considering both molecular interactions and size differences leads to deviations from the Langmuir equation in opposite directions. Therefore, the typically good fit of the Langmuir equation for surfactant adsorption isotherms is often coincidental [14].

Equation 2.7 can be used to represent Langmuir's model:

$$\Gamma = \frac{\Gamma_\infty k_L}{1 + k_L C} \tag{2.7}$$

where Γ is the surface coverage of the adsorbate, Γ_∞ is the maximum surface coverage, k_L is the Langmuir constant, and C is the adsorbate concentration [16].

2.3.4 Wettability and contact angle

Wetting refers to a liquid's ability to spread across a surface, which may be either a solid or another immiscible liquid. The extent of wetting, known as wettability, is determined by the characteristics of both the liquid and the surface. Wettability is influenced by the balance between adhesive forces (between the liquid and the surface), which promote wetting, and cohesive forces (within the liquid itself), which oppose wetting. When a droplet is placed on a solid surface, it may spread out, thereby increasing the liquid–solid and liquid–air interfacial areas, while the solid–air interface decreases. This results in a reduction in the contact angle (θ_c) between the droplet and the surface. A low contact angle indicates that the liquid spreads easily, suggesting the surface is hydrophilic. In contrast, a contact angle near or above 90° indicates a hydrophobic surface. If the contact angle exceeds 150°, the surface is classified as superhydrophobic [17]. Surfactants increase the

wetting of liquids on surfaces by reducing surface tension.

The contact angle of a liquid droplet on a flat, solid surface has traditionally been measured using a sessile drop method, where the droplet rests on a horizontal surface. A goniometer is employed for this purpose, and the contact angle is observed and measured directly using a microscope objective to accurately view the angle [17].

2.3.5 Clouding phenomena

One notable characteristic of non-ionic surfactants, in contrast to other surfactant types, is that their solubility decreases as temperature increases. A common observation is that, upon heating, a solution containing a non-ionic surfactant begins to scatter light strongly within a specific temperature range, resulting in a "cloudy" appearance. This cloudiness marks the beginning of phase separation. This results from a specific characteristic of the phase diagram. The isotropic solution region is bordered towards higher temperatures by the lower cosolute curve, beyond which the system undergoes phase separation into a surfactant-rich phase and a surfactant-poor phase. The temperature at which this phase separation occurs is known as the cloud point. Aqueous solutions of various non-ionic surfactants display clouding phenomena when heated or cooled, and this behavior is influenced by the type and concentration of the amphiphiles. Cloud point measurements are typically carried out with 1 wt% concentration of surfactants in solution and phase separation is detected through visual observation [18, 19].

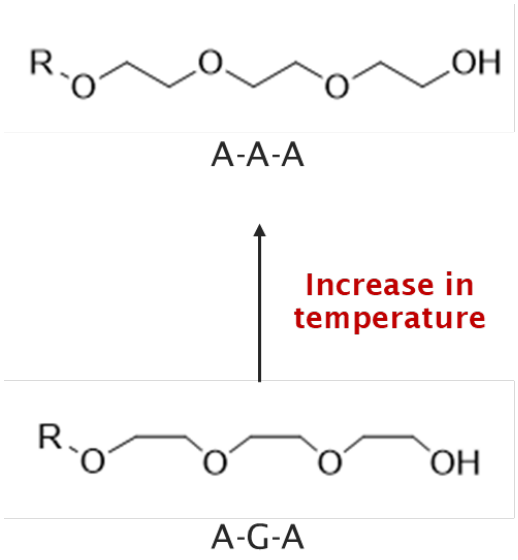

Figure 2.5: Conformational change in polyoxyethylene chains from anti-gauche-anti (A-G-A) to anti-anti-anti (A-A-A) with increase in temperature.

A polyoxyethylene chain can adopt numerous conformations, each with varying energy levels. The most stable, low-energy conformation (anti-gauche-anti) occurs

when the oxyethylene group is in the gauche configuration around the C–C bond and anti around the C–O bond. This conformation, which predominates at lower temperatures, possesses a large dipole moment. However, it has a low statistical probability. As temperature increases, higher-energy conformations with greater statistical weight become more prevalent. These include structures such as the anti–anti–anti conformation, which possess smaller or negligible dipole moments. As a result of these conformational shifts, polyoxyethylene chains become progressively less polar with rising temperature. This reduced polarity diminishes their interaction with water (leading to lower hydration) and enhances their interactions with each other. Consequently, this promotes tighter packing of the head groups in surfactant self-assemblies and increases the likelihood of phase separation into a more concentrated phase [20]. The conformational change with increase in temperature is depicted in Figure 2.5.

Polyglycerol-based surfactants do not possess the same conformations as polyethylene-based surfactants. Therefore, the reasons for clouding behavior may be different.

2.3.5.1 Effect of salt addition on solubility

The phenomenon of clouding is significantly influenced by the presence of various cosolutes, for example, inorganic salts [19]. Specific ion effects have attracted significant attention since the groundbreaking work of F. Hofmeister. The Hofmeister (or Lyotropic) series classifies ions based on their kosmotropic or water-structuring tendencies. This classification ranks ions according to their ability to promote the salting-out effect [21].

For anions:
$SO_4^{2-} > HPO_4^{2-} > OH^- > F^- > HCOO^- > CH_3COO^- > Cl^- > Br^- > NO_3^- > I^- > SCN^- > ClO^-$.

For cations:
$Al^{3+} > Mg^{2+} > Ca^{2+} > Li^+ > H^+ > Na^+ > K^+ > Cs^+ > NH_4^+ > (NCH_3)_4^+$.

Ions positioned toward the left of the series are commonly referred to as salting-out agents, kosmotropes, or water structure makers. In contrast, those on the right are known as salting-in agents, chaotropes, or water structure breakers. Initially, this classification was based on the ions' affinity for water, often described as their water-withdrawing power. Interestingly, the Hofmeister series also correlates with various other ion properties, such as hydration level, atomic radius, and polarizability. Typically, salting-out ions exhibit higher hydration and lower polarizability compared to salting-in ions. Consequently, specific ion effects, as described by the Hofmeister series, also influence processes like surfactant micellization. The Hofmeister series was originally proposed to explain the influence of salts on proteins, but it was later extended to apply to colloidal systems, including those involving surfactants. Research has demonstrated that micellar characteristics, such as the CMC, as well as the shape and size of

surfactant aggregates, are influenced not only by the properties of the surfactant itself but also by the specific ions with which it interacts [21].

2.3.5.2 Relationship between solubility and critical packing parameter

The critical packing parameter (CPP) is a dimensionless number that relates the hydrophilic area (a), the extended length (l_{max}), and the hydrophobic volume (v) of a surfactant, as illustrated in Figure 2.6 [22]. The calculation of the CPP is given by Equation 2.8:

$$CPP = \frac{v}{(al_{max})} \tag{2.8}$$

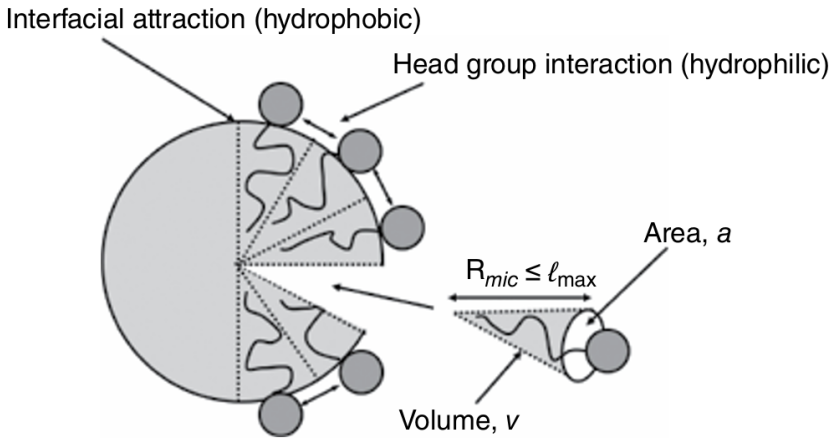

Figure 2.6: The CPP provides a relationship between head group area, extended length, and a surfactant's hydrophobic volume [22].

Based on the Fontell scheme (Figure 2.7), it can be observed that surfactants with a critical packing parameter (CPP) of less than 1/3—typically single-chain surfactants with highly polar head groups, such as ionic surfactants in the absence of electrolytes—tend to form spherical micelles. This category also includes nonionic surfactants with large head groups. When the CPP falls in the range of 1/3 to 1/2, rod-like micellar structures are usually formed. This behavior is seen in single-chain ionic surfactants with added electrolytes, those with strongly bound counterions, or nonionic surfactants with moderately sized head groups. Higher CPP values are generally associated with double-chain amphiphiles or nonionic surfactants possessing relatively small head groups [22].

The CPP has not only a geometrical aspect, but also an aspect of interactions. In a dilute regime, two surfactants are relatively far from each other, and the only interactions between their hydrophobic tails are van der Waals interactions. However, at higher concentrations (for instance, at or above the CMC), surfactant molecules are closer to each other. In this case, hydrophobic interactions occur between the tails, and interactions also occur between the head groups. Since the

polyglycerol head group consists of hydroxyl functional groups, the possibility of hydrogen bonding arises. Hydrogen bonding can occur between head groups and also between a head group and surrounding water molecules. Additionally, when surfactant molecules come closer to each other, the water between them gets displaced. However, water still exists in the remaining surroundings. Salt addition affects interactions, in turn altering the CPP of polyglycerol-based surfactants. The addition of a chaotrope disrupts structured water, making the surfactant more available to interact with water. This leads to increased hydration of the head group, decreasing the CPP, and consequently improving surfactant solubility. On the other hand, the addition of a kosmotrope promotes interactions between water molecules, making them less available to interact with the surfactant. This leads to dehydration of the head group, increasing the CPP, resulting in reduced solubility.

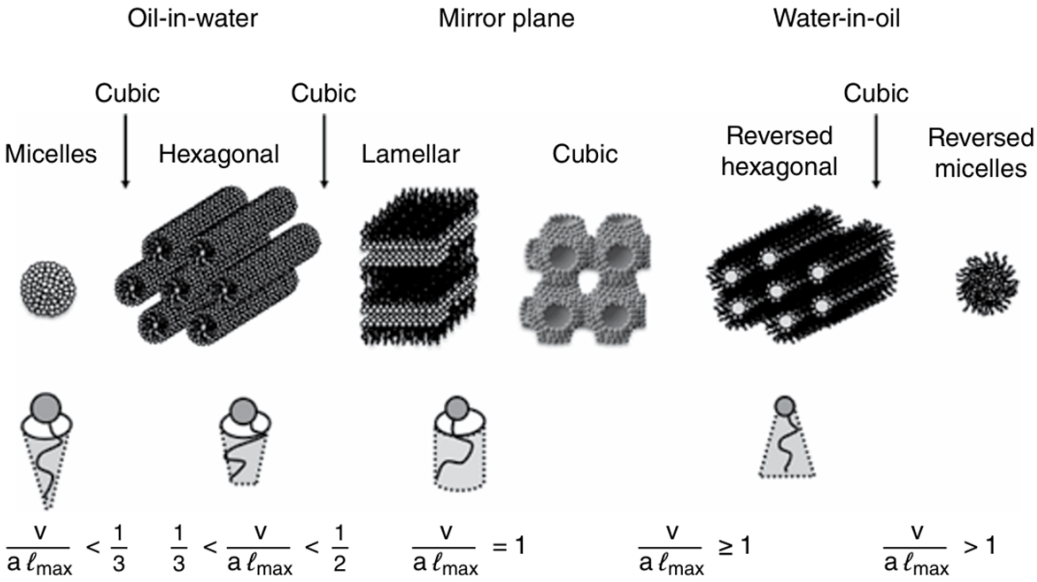

Figure 2.7: Fontell scheme, illustrating the CPP and preferred aggregate structures of surfactant molecules [22].

2.3.5.3 Alkaline hydrolysis of esters

Alkaline hydrolysis (or saponification) is a reaction which involves breaking down a chemical bond (in this case, ester bond) in the presence of a base (such as NaOH), resulting in a carboxylic acid or carboxylate, and an alcohol. Using this process, it is possible to solubilize esters that are sparingly soluble in water. When NaOH is added to an aqueous solution of PGEs, the products obtained are polyglycerol and sodium salts of fatty acids.

2.4 Application in cleaning formulations

Detergents are chemical formulations designed to provide cleaning capabilities on specific surfaces. Their cleaning action typically involves two main steps: first,

detaching soil or dirt from surfaces such as textiles or ceramics, and second, dispersing the removed soil into the washing liquid. Detergents are widely used in both household and industrial/institutional cleaning applications. These formulations primarily consist of surfactants, with additional components such as hydrotropes, chelating agents, and pH-adjusting acids or bases present in smaller quantities. Surfactants play a crucial role by promoting surface wetting and reducing surface tension, making it easier to lift and remove soil. They also stabilize the dispersed soil. Chelating agents are used to take care of the metal ions present in hard water, such as Mg^{2+} and Ca^{2+}. Hydrotropes are used to solubilize the surfactant, which are often more effective when very hydrophobic. Formulations are carefully tailored by selecting specific ingredients to achieve the desired cleaning performance for different surface types [23].

One class of detergents is hard surface cleaners. The term "hard surface" refers to surfaces that are generally resistant to solid penetration and do not readily absorb liquids. These are commonly found in homes and industrial settings and include materials such as tile, stone, marble, ceramics, metal sinks, pots, and kitchen appliances made of porcelain or metal. Hard surface cleaners are specially formulated to effectively clean soiled surfaces, often without the need for rinsing. Key performance expectations from these products include rapid wetting, efficient emulsification of dirt, and minimal residue such as streaks or greasy films after cleaning. These cleaners are manufactured for both household and institutional/industrial use. Household hard surface cleaners are usually gentle on the skin, feature pleasant fragrances, and are formulated to have low or no toxicity. In contrast, industrial or institutional formulations are more powerful and fast-acting, with less emphasis on skin sensitivity or irritation [23].

3
Methods

The details of the synthesis of PGEs, the methods used for their characterization and application in cleaning formulations are explained in this chapter.

3.1 Solvent-free synthesis

Three batches of surfactants were synthesized using different reactant molar ratios and reaction conditions with the aim of obtaining a higher fraction of monoesters in the product. All three syntheses were performed by reacting an excess of polyglycerol-3 with decanoic acid in the presence of p-toluenesulfonic acid (PTSA) monohydrate catalyst at high temperature and low pressure. An excess of polyglycerol-3 was used to promote the formation of monoesters.

Figure 3.1 illustrates the reaction and reaction conditions for batch PG3C10_2:1a. Figure 3.2 illustrates the reaction and reaction conditions for batches PG3C10_2:1b and PG3C10_10:1. Although the reactions depict a linear molecule as the product, in practice, a polydisperse mixture of esters is formed. Unreacted polyglycerol is also present in the product.

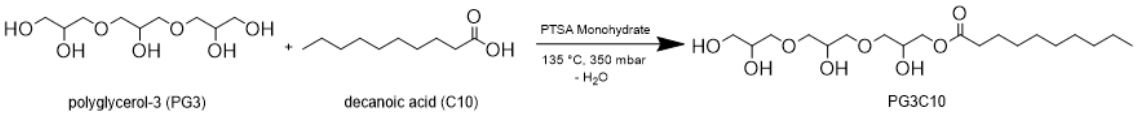

Figure 3.1: Reaction between polyglycerol-3 and decanoic acid with reaction conditions for batch PG3C10_2:1a.

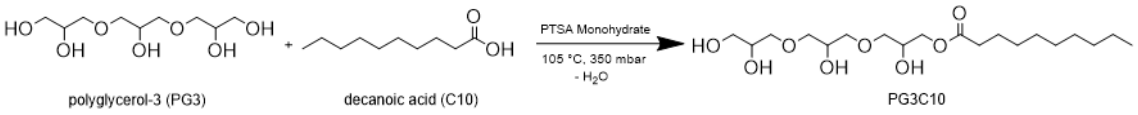

Figure 3.2: Reaction between polyglycerol-3 and decanoic acid with reaction conditions for batches PG3C10_2:1b and PG3C10_10:1.

Polyglycerol-3 and decanoic acid were added to a 500 mL round bottom flask, which was then placed in a silicone oil bath. The mixture was heated to 70 °C to melt the decanoic acid and to lower the viscosity of polyglycerol-3 to facilitate stirring.

Once this was achieved, PTSA catalyst was added and the temperature was set to the desired reaction temperature. The pressure was lowered from 800 mbar to 550 mbar. Once the reaction temperature was reached, the pressure was lowered to reach a value of 350 mbar. The reaction was left undisturbed for 18 hours (counted from when the catalyst was added). Upon completion of the reaction, the product was transferred to glass vials for storage. The reaction parameters for the synthesis of the three batches are given in Table 3.1. Further details are given in Table A.1 in Section A.1.

Table 3.1: Reaction parameters for PGEs synthesized through the solvent-free route.

Batch	Molar ratio of polyglycerol-3 to decanoic acid	Molar ratio of PTSA catalyst to decanoic acid	Reaction temperature (°C)
PG3C10_2:1a	2	0.098	135
PG3C10_2:1b	2	0.01	105
PG3C10_10:1	10	0.01	105

3.1.1 Determination of reaction conversion

Volumetric titration was performed for the surfactants synthesized through the solvent-free route to determine the conversion of the reaction, i.e., to determine how much unreacted fatty acid was present after synthesis. Each sample was prepared by adding 0.5 g of surfactant, 25 ml of ethanol, and 25 ml of Milli-Q water in a beaker. The mixture was allowed to stir continuously throughout the entire titration. A Jenway 3510 pH meter was used to measure the pH. The sample solution was titrated against a solution of 0.0079 M KOH and the pH was noted until it reached 10 - 11. A curve of pH versus volume of KOH solution was plotted and the percentage of conversion was calculated using the equivalence point.

3.1.2 Removal of unreacted polyglycerol

The purification of the surfactants synthesized through the solvent-free route was performed by liquid extraction to remove excess (unreacted) polyglycerol from the product mixtures. DCM was identified as the suitable solvent for the three batches. The optimal quantities of product mixture and DCM required for efficient extraction were unknown, so the process was carried out by trial and error. Certain amounts of product mixture (product of synthesis) and DCM were added to a round bottom flask and stirred. The details for each batch are included in Table 3.2 and Table 3.3. The mixture was then transferred to a separation funnel, where it was allowed to sit until the separation of the phases was visible. Since DCM is more dense than polyglycerol, the polyglycerol phase is separated at the top. The bottom phase, consisting of DCM and esters, was allowed to flow out of the funnel and was transferred to a round bottom flask. The top phase was also transferred to another flask. The DCM was then evaporated from both phases using a rotary evaporator. Two extractions were performed for batches

PG3C10_2:1a and PG3C10_10:1, where the bottom phases of the first extractions were used during the second (or refined) extractions.

Table 3.2: Details of the first extraction process.

Batch	Amount of product mixture (g)	Amount of DCM (g)	Stirring time (min)
PG3C10_2:1a_E1	3.27	50.19	190
PG3C10_2:1b_E1	3.21	52.47	60
PG3C10_10:1_E1	11.89	27.81	40

Table 3.3: Details of the refined extraction process.

Batch	Amount of product mixture (g)	Amount of DCM (g)	Stirring time (min)
PG3C10_2:1a_E2	0.05	10.15	60
PG3C10_10:1_E2	0.90	2.87	60

The addition of too much DCM was avoided because polyglycerol may have an affinity for DCM and dissolve in it, which would have lowered the purity of the product. A larger quantity of surfactant and a smaller quantity of DCM were used specially for the extraction of PG3C10_10:1 because the ratio of polyglycerol to fatty acid was much greater (molar ratio of 10) than for PG3C10_2:1a and PG3C10_2:1b (molar ratio of 2), meaning that the amount of pure surfactant present in the mixture was relatively lower. The purpose was also to avoid the dissolution of too much polyglycerol in the bottom phase.

3.2 Synthesis in solvent

Five batches of surfactants were synthesized using a 1:1 molar ratio between polyglycerol and acyl chloride in the presence of N, N - dimethylformamide (DMF) as the solvent. Both polyglycerol and acyl chloride are soluble in DMF, resulting in a one-phase system during synthesis. 2 molar equivalents of pyridine (base) were added to neutralize the formed hydrochloric acid and to facilitate completion of the reaction. A mixture of acyl chloride and DMF was taken in an addition funnel and was added dropwise to a mixture of polyglycerol, pyridine, and DMF to promote monoester formation. All reactions were performed at room temperature (23 °C), for a duration of 22 hours. The five surfactant synthesis reactions are illustrated in Figure 3.3. Upon completion of the reaction, DMF was evaporated using a rotary evaporator. To further remove traces of DMF and pyridine, the product mixture was connected to a Schlenk line overnight. The product was then transferred to a glass vial. ^{1}H NMR was employed to calculate the purity of the synthesized surfactants.

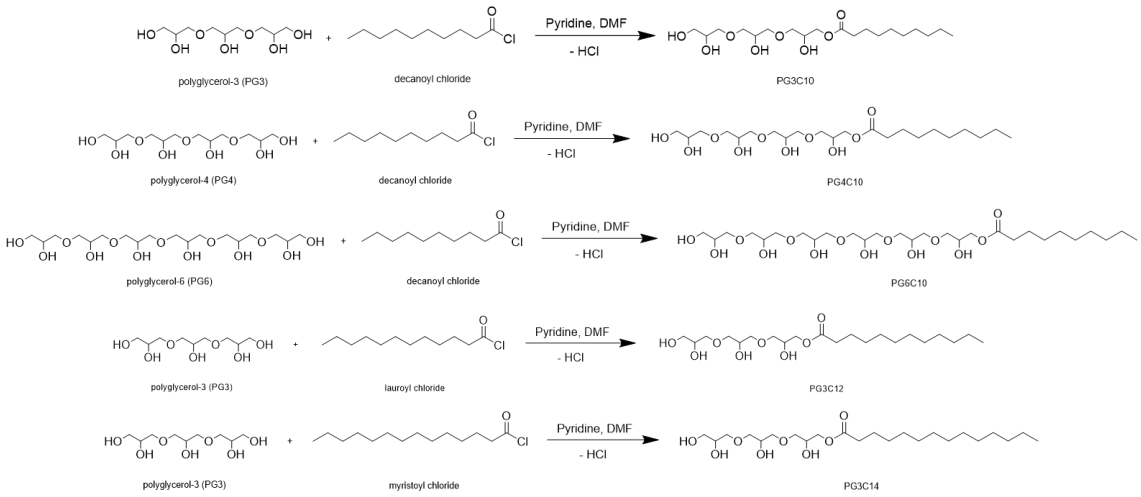

Figure 3.3: Synthesis reactions for PG3C10, PG4C10, PG6C10, PG3C12 and PG3C14 (from top to bottom).

3.3 Characterization

3.3.1 Liquid Chromatography-Mass Spectrometry

The compositions of the surfactant batches were analyzed by performing LC-MS measurements using an Agilent 1100-Series LC connected to an Agilent 6550 QTOF Mass Spectrometer. The samples were loaded using dilute methanol solution. Limits were set such that if a component was present in a quantity below that limit, the result would show 0%.

A targeted qualitative analysis was performed against a database of targeted compounds. This database consisted of sum formulas of interest and their corresponding exact masses and names. The target compounds were polyglycerols (n=1-10), the same polyglycerols that had lost 1, 2, or 3 equivalents of water due to cyclization / elimination reactions, fatty acids (C10, C12 and C14), their corresponding mono-, di-, and triesters with the polyglycerols, and solvents / catalysts used in the reactions.

3.3.2 Infrared Spectroscopy

Single drops of the synthesized surfactants were placed on the surface of the crystal such that it was fully covered. They were then scanned using a PerkinElmer FTIR spectrometer and the resulting spectra were analyzed using OriginPro. All measurements were performed in the middle IR range, from 450 cm^{-1} to 4000 cm^{-1}.

3.3.3 Nuclear Magnetic Resonance spectroscopy

Samples were prepared by dissolving 0.01 g of surfactant in 600 μl of methanol-d4. Both ^{1}H NMR and ^{13}C NMR were performed on the samples and the resulting

spectra were analyzed using the MestReNova software (version 15.0.1).

3.3.4 Pendant drop tensiometry

Stock solutions of 0.7 wt%, 1 wt%, 2 wt% and 3 wt% were prepared in Milli-Q water for each surfactant. Stock solutions of 1 wt% and 3 wt% were prepared for polylycerol-3. These stock solutions were then diluted to create a logarithmic concentration series. These concentrations are represented in Tables A.1, A.2 and A.3 in Section A.2. The tensiometry measurements were performed using a Biolin Scientific Attension Theta optical goniometer. 5 - 8 drops were recorded for each solution. The drops were allowed to stabilize for 30 seconds before the instrument recorded them for 2 seconds at 15 frames/second. OneAttension software (version 2.6.0.0) was used to automatically calculate the surface tensions during the recordings. Curves of surface tension against surfactant concentration were plotted on a logarithmic scale to determine the surface tensions and the CMC values of the surfactants. A similar plot was created for polyglycerol-3 to check if it had any effect on surface activity and properties of the surfactants. The mean surface tension value from the 5-8 drops was considered for plotting the curves. Langmuir and Gibbs adsorption isotherms were used for fitting the curves for the calculation of surface excess concentration (Γ) and area per molecule (A) of the surfactants. The fit of the data points to the Langmuir isotherm was done with an optimization function which uses a non-linear least-squares curve fit.

Since the solvent-free synthesis was done with an excess of polyglycerol-3, the ST curves of the surfactants before extraction (or surfactant mixtures) were not representative of the actual surfactants. Therefore, the expected fractions of surfactant in the mixtures were calculated and the ST curves for the actual surfactant were predicted. This was done under two assumptions: (i) only monoesters were present, and (ii) the conversion of the reaction was 100%. After extraction, pendant drop tensiometry was performed on the three batches. Curves of surface tension against the actual surfactant concentration were plotted and compared with the predicted ST curves.

3.3.5 Cloud point measurements

1 wt% solution of the surfactant was prepared in Milli-Q water and transferred to a test tube. The test tube was placed in a water bath and heated from room temperature to 85 °C. The temperature at which phase separation occurred was noted. The solution was then cooled and the temperature at which there was a change in clouding behavior was noted.

3.3.6 Addition of salts to surfactant solutions

The solubility aspect of the surfactants was investigated through the addition of two salts, namely, NaF (kosmotrope) and NaSCN (chaotrope). 1 mL of 1 wt% surfactant solution was taken in 6 vials. The first vial contained surfactant solution without salt. This was used as a reference to compare and assess the

effect of salt addition on surfactant solubility. Varying volumes of 0.5 M NaF solution were added to the other 5 vials, resulting in a set of solutions with different ionic concentrations: 0.024 M, 0.045M, 0.065M, 0.083 M, and 0.1 M. The same procedure was followed for the addition of 0.5 M NaSCN solution.

To account for possible dilution effects, which could result in incorrect visual interpretation, another set of tests was conducted. 200 μL of 1 wt% surfactant solution and 1 mL of Milli-Q water were added to a vial. In another vial, 200 μL of 1 wt% surfactant solution and 1 mL of 0.5 M NaF solution were taken. This ensured that the concentrations of both solutions (with and without salt) were similar. The same procedure was followed for the addition of 0.5 M NaSCN solution.

3.3.7 Alkaline hydrolysis of PGEs using NaOH

1 mL of 1 wt% PG3C10 solution was taken in 7 vials. The first vial contained surfactant solution without salt. This was used as a reference to compare and assess the effect of salt addition on surfactant solubility. Varying volumes of 1 M NaOH solution were added to the other 6 vials, resulting in a set of solutions with different molar ratios of NaOH to PG3C10 ester. The details are given in Table 3.4. The solutions were placed in an oven at 60 °C for 24 hours. They were then kept for another 24 hours at a higher temperature of 70 °C to promote hydrolysis.

Table 3.4: Details of NaOH addition to 1 mL of 1 wt% PG3C10 solutions.

Vial	Volume of NaOH added (μL)	Molar ratio of NaOH to PG3C10 ester
1	0	0.0
2	20	0.8
3	25	1.0
4	50	2.0
5	75	3.0
6	87	3.5
7	90	4.0

3.4 Application of the synthesized PGEs in cleaning formulations

The cleaning formulations were prepared with the following components: 1 wt% prmary surfactant, 1 wt% chelating agent, an auxiliary surfactant/hydrotrope, and Milli-Q water. The primary surfactants in these formulations are the synthesized PGEs. The chelating agent used was 47 wt% Tetrasodium Glutamate Diacetate (GLDA-Na_4), which contains four carboxyl groups that form bonds with divalent and trivalent ions in hard water. The hydrotrope used was 40 wt% Sodium Xylene Sulfonate (SXS), which is minimally surface active, solubilizes the PGEs, and

makes the formulation transparent.

Soil was applied to the surfaces of ceramic plates to mimic dirt on kitchen surfaces. The soil was left to age overnight to ensure that it remained firmly on the surfaces of the plates. After aging, the plates were ready to be used to test the cleaning efficacy of the formulations. 10 mL of each formulation was poured onto the soiled plate and allowed to act for 60 seconds to allow enough time for the surfactants to adsorb onto the surface. The plates were then rinsed with tap water.

The compositions of the formulations are given in Table 3.5 and Table 3.6. A greater amount of SXS was required for the more hydrophobic surfactants since they were more difficult to solubilize. All formulations, except for PG3C14, turned completely transparent upon the addition of SXS.

Table 3.5: Compositions of formulations of the surfactants synthesized through the solvent-free route.

Surfactant batch	Surfactant (wt%)	GLDA-Na_4 (wt%)	SXS (wt%)	Milli-Q water (wt%)
PG3C10_2:1a	1.02	0.98	7.84	90.16
PG3C10_2:1b	1.00	1.04	18.61	79.35
PG3C10_10:1	1.01	0.99	2.89	95.11

Table 3.6: Compositions of formulations of the surfactants synthesized through the solvent route.

Surfactant batch	Surfactant (wt%)	GLDA-Na_4 (wt%)	SXS (wt%)	Milli-Q water (wt%)
PG3C10	1.03	1.04	15.48	82.45
PG4C10	1.00	1.06	5.59	92.35
PG6C10	0.98	1.05	0.51	97.46
PG3C12	1.00	1.18	34.02	63.80
PG3C14	0.99	0.97	40.80	57.24

3.4.1 Contact angle measurements

Contact angles were measured to evaluate the wettability of the formulations. A glass slide with paraffin wax (hydrophobic surface) was taken as the substrate for all experiments. The measurements were performed using a Biolin Scientific Attension Theta optical goniometer. 2 drops were recorded for each formulation. The contact angles were recorded for 60 seconds at 3.8 frames/second from the moment the drop landed on the surface of the paraffin wax. OneAttension software (version 2.6.0.0) was used to automatically calculate the mean of the left and right contact angles during the recordings. Curves of contact angle against time were plotted to analyze the rate of adsorption, wettability, and the contact angle of the formulations at 60

seconds, which is the amount of time the formulations were allowed to remain on the soiled plates before rinsing. The mean contact angle value from two drops was considered.

4

Results and discussion

The results of synthesis, characterization, and cleaning applications of the surfactants are discussed in this chapter.

4.1 Surfactants synthesized through the solvent-free route

During synthesis, observations were made over time (t) for the three batches. These are shown in Figures 4.1, 4.2 and 4.3. Upon the addition of the catalyst, a color change was observed for PG3C10_2:1a (Figure 4.1 (c)). This could be due to a side reaction occurring at high temperature. For PG3C10_2:1b, no such color change was observed. As can be seen in Figure 4.2 (d), the final product was colorless, while that for PG3C10_2:1a was dark brown (Figure 4.1 (d)). This means that the reaction temperature had a significant impact on the color of the surfactant mixtures, as PG3C10_2:1a was synthesized at higher temperature. There was no change in the appearance of PG3C10_10:1 over time (Figure 4.3). From Figure 4.3 (c), it can be seen that the product was colorless. This is because the reaction was performed at a lower temperature, similar to PG3C10_2:1b.

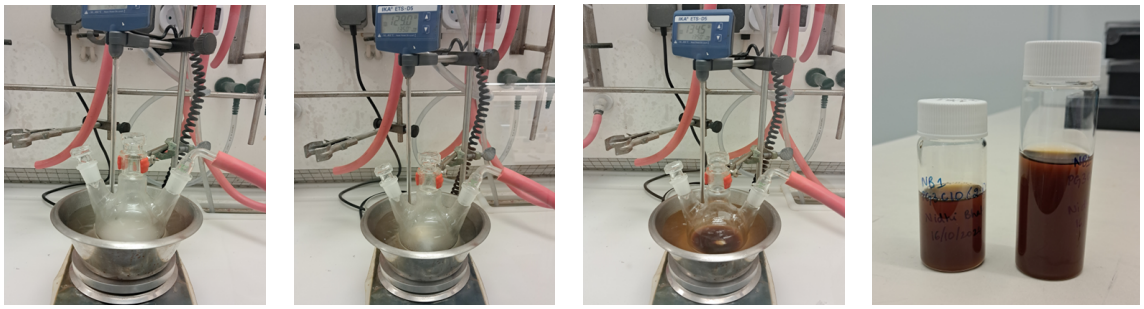

(a) **(b)** **(c)** **(d)**

Figure 4.1: Appearance of PG3C10_2:1a throughout the reaction, (a) translucent mixture at t = 20 min, (b) transparent mixture at t = 30 min, (c) dark brown mixture at t = 18 h, (d) highly viscous, dark brown product.

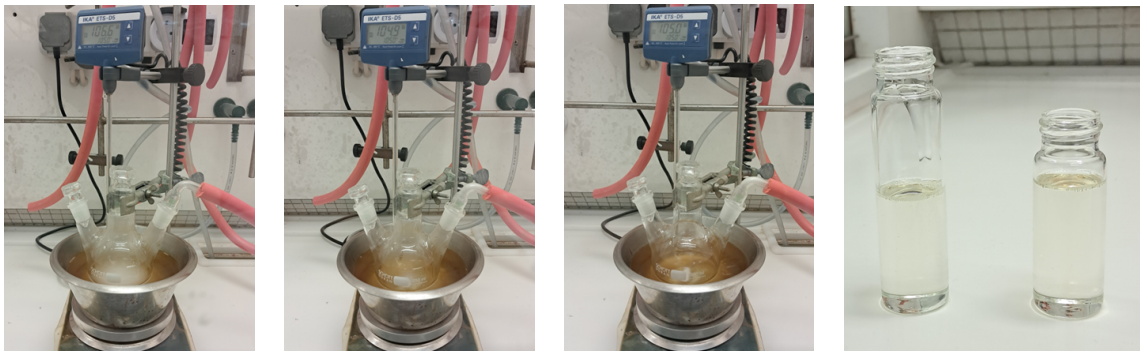

(a) (b) (c) (d)

Figure 4.2: Appearance of PG3C10_2:1b throughout the reaction, (a) translucent mixture at t = 40 min, (b) transparent mixture at t = 80 min, (c) transparent mixture at t = 18 h, (d) highly viscous, colorless product.

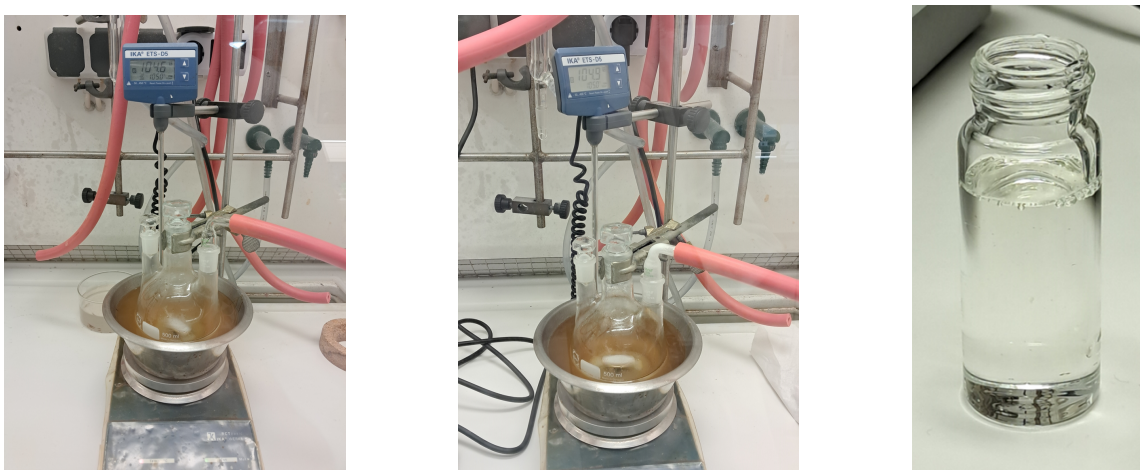

(a) (b) (c)

Figure 4.3: Appearance of batch PG3C10_10:1 throughout the reaction, (a) transparent mixture at t = 0 min, (b) transparent mixture at t = 18 h, (c) highly viscous, colorless product.

The titration curves for the synthesized surfactants are shown in Figure A.1 in Section A.3. Based on the locations of the equivalence points, the conversions were determined to be 99%, 99%, and 97% for PG3C10_2:1a, PG3C10_2:1b and PG3C10_10:1, respectively. Thus, it was concluded that there was hardly any free fatty acid present in the products.

The surfactant yields obtained after extraction are given in Table 4.1. The surfactant yield (%) represents the fraction of surfactant yield (g) to the amount of product mixture (g) (given in Table 3.1 and Table 3.2). The yield for PG3C10_10:1 was lower due to the large amount of unreacted polyglycerol present in the product mixture. The mass of the starting material for the refined extraction is the surfactant yield (g) obtained after the first extraction, i.e., the mass of the bottom phase of the first extraction.

Table 4.1: Surfactant yields after the extraction process.

Batch	Yield after the first extraction (g)	Yield after the refined extraction (g)	Yield after the first extraction (%)	Overall yield after the refined extraction (%)
PG3C10_2:1a	1.62	0.04	49	39
PG3C10_2:1b	1.68	N/A	52	N/A
PG3C10_10:1	1.70	0.77	14	12

4.1.1 Surfactant composition analysis using LC-MS

LC-MS was performed to determine the composition of the surfactant mixtures, i.e., the amount of the polyglycerol, monoesters, diesters and triesters. The results obtained are an approximation and they are listed in Table 4.2. The data for the samples after extraction is for the bottom phases (surfactant-rich). PG3C10_2:1a_E2 and PG3C10_2:1b_E1 had a greater fraction of diesters and triesters, whereas PG3C10_10:1_E1 contained more monoesters. It was concluded that the refined extraction did not have much of an effect on the removal of polyglycerol for PG3C10_2:1a. A refined extraction was not carried out for PG3C10_2:1b since it was synthesized using the same molar ratio of reactants as PG3C10_2:1a.

The percentages of monoesters to total esters were calculated and the approximate values are listed in Table 4.3. The reduction in monoester content in the bottom phase after extraction could be due to the affinity of monoesters towards polyglycerol, meaning that some of the monoesters escaped into the top phase (polyglycerol-rich). This can be observed in the LC-MS results shown in Table 4.4, where the esters present in the top phase are predominantly monoesters.

Table 4.2: Compositions of the surfactants before and after extraction.

Batch	Polyglycerol	Monoester	Diester	Triester
PG3C10_2:1a	33%	41%	20%	6%
PG3C10_2:1a_E1	11%	53%	29%	7%
PG3C10_2:1a_E2	10%	53%	29%	8%
PG3C10_2:1b	37%	35%	22%	6%
PG3C10_2:1b_E1	7%	48%	35%	10%
PG3C10_10:1	81%	16%	2%	1%
PG3C10_10:1_E1	15%	68%	15%	2%

Table 4.3: Percentages of monoesters to total esters derived from the LC-MS data of the surfactants.

Batch	Monoesters/total esters
PG3C10_2:1a	61%
PG3C10_2:1a_E1	60%
PG3C10_2:1a_E2	59%
PG3C10_2:1b	55%
PG3C10_2:1b_E1	51%
PG3C10_10:1	93%
PG3C10_10:1_E1	80%

Table 4.4: Compositions of top phases (polyglycerol-rich) of the three batches after the first extraction.

Batch	Polyglycerol	Monoester	Diester	Triester	Monoesters/total esters
PG3C10_2:1a	93%	7%	0%	0%	100%
PG3C10_2:1b	97%	3%	0%	0%	100%
PG3C10_10:1	96%	4%	0%	0%	100%

4.1.2 Qualitative analysis using IR spectroscopy

IR spectroscopy was performed on the three batches of surfactants after the first extraction. This was done for qualitative analysis. Figure 4.4 and Figure 4.5 show the spectra of the surfactant-rich and the polyglycerol-rich phases after extraction, respectively. In Figure 4.4, the intense peak at 1735 - 1740 cm^{-1} represents the carbonyl group, indicating that the sample contained esters. This is the peak that confirms the presence of esters. A peak at around 735 cm^{-1} was observed, which is from residual DCM that was not removed during rotary evaporation. The peak disappeared after the DCM was evaporated completely. In Figure 4.5, although the peak at 1735 - 1740 cm^{-1} is present, it is not intense. This means that the top phase did not contain many esters. The peak at around 735 cm^{-1} is the residual DCM. The spectrum of polyglycerol-3 is also included and it is evident that the top phases correspond to this compound.

4.1.3 Quantitative analysis using NMR spectroscopy

NMR spectroscopy was performed on the three batches of surfactants after the first extraction. Upon analysis of the spectra with respect to the chemical shifts of the peaks, it was concluded that the desired PGEs were formed during synthesis. It was observed that the intensity of the peaks of the fatty acid increased after extraction, meaning that extraction removed a significant amount of polyglycerol from the three batches, yielding purer surfactants. The top phases predominantly contained polyglycerol. The ^{1}H NMR and ^{13}C NMR spectra for the surfactants

before and after the first extraction are given in Section A.4, along with details of the peak positions and integrals.

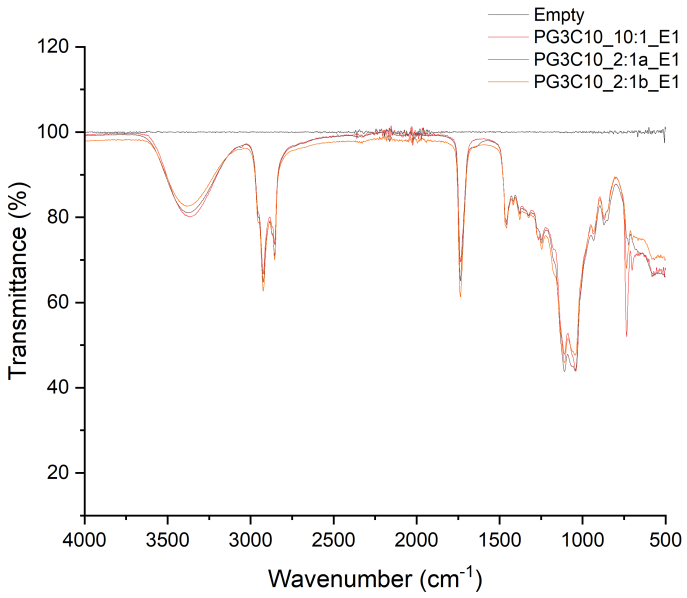

Figure 4.4: IR spectra of the surfactants (bottom phases) after the first extraction.

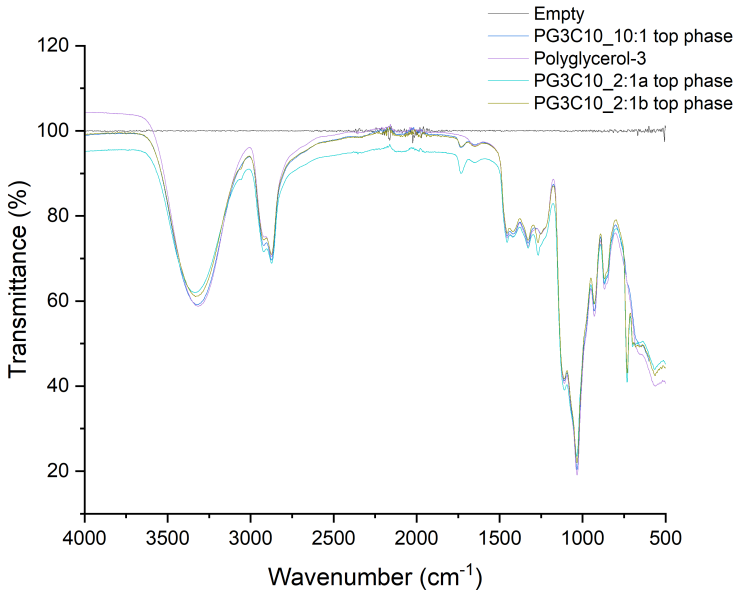

Figure 4.5: IR spectra of polyglycerol-3 and the top phases after the first extraction.

4.1.4 Effect of monoester content on surface properties

Since the surfactants contained unreacted polyglycerol prior to extraction, the expected concentrations of pure surfactant were calculated to create ST curves based on the assumptions stated in Section 3.4.4. The expected fractions of surfactant in the product mixture were 0.62, 0.62 and 0.15 for PG3C10_2:1a, PG3C10_2:1b and PG3C10_10:1, respectively. These fractions were multiplied with the concentrations of the logarithmic series of these surfactants, which are listed in Table A.1 in Section A.1. The ST curves are shown in Figure 4.6. The ST curves of the surfactants after the first extraction are shown in Figure 4.7.

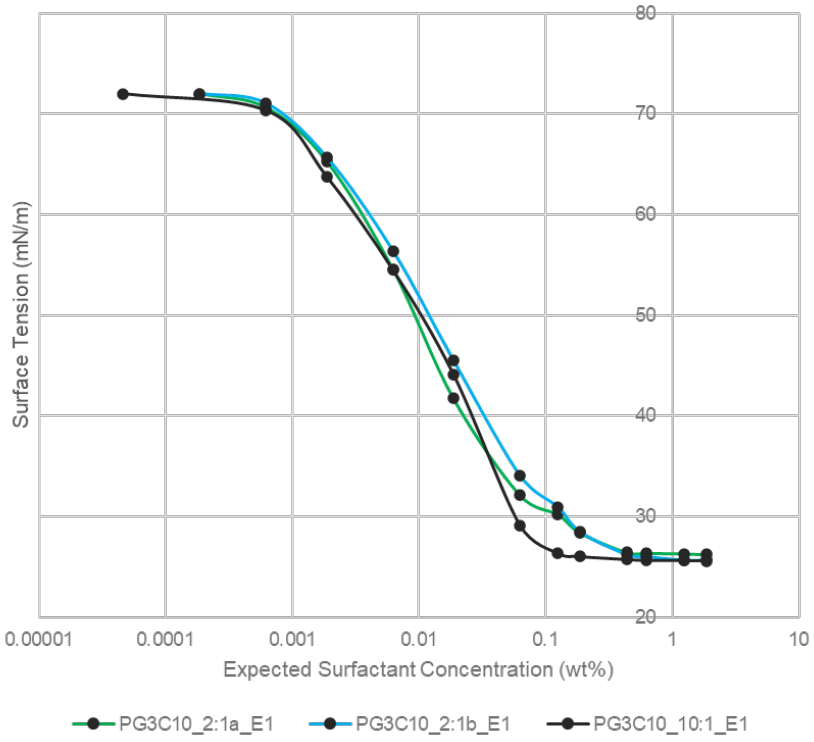

Figure 4.6: Logarithmic plot of surface tension (mN/m) versus expected surfactant concentration (wt%).

The surface tension versus concentration for polyglycerol-3 was measured to check if it had any surface properties. This graph is presented as Figure A.8 in Section A.5. It was concluded that polyglycerol-3 has minimal surface activity at concentrations below 3 wt%.

Table 4.5 shows the values of ST at the plateau, CMC, surface excess concentration, and area per molecule, which were obtained from the ST curves in Figure 4.6. Table 4.6 shows the CMC values for the surfactants after the first extraction, obtained from the ST curves in Figure 4.7. The ST values, the surface excess concentration, and the area per molecule were the same as the predicted values, with only CMC values varying. It can be seen from Table 4.6 that the CMC values of the surfactants were higher than those expected. The surface tensions of all the surfactants were quite low at the plateau, implying good surface

activity.

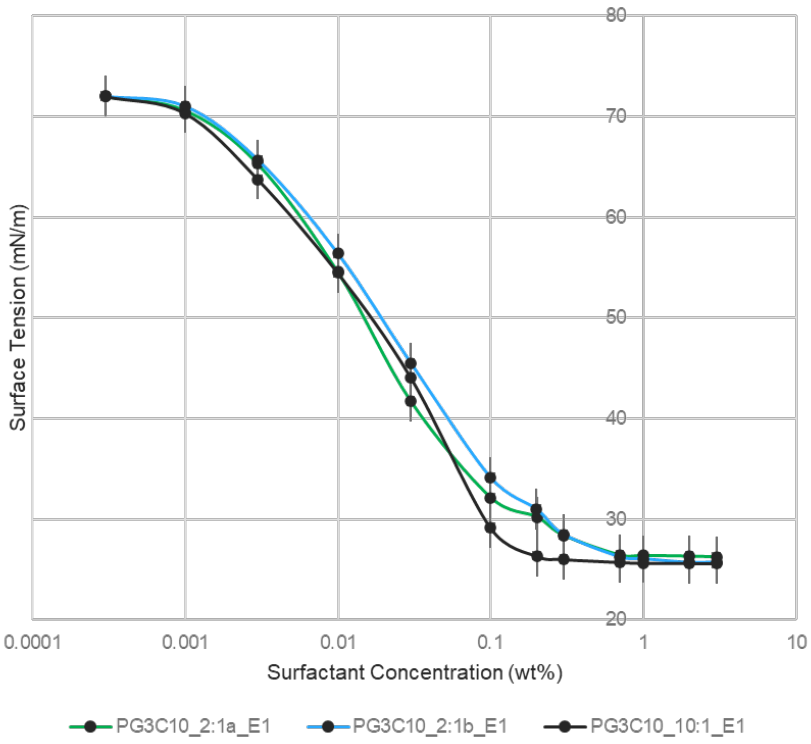

Figure 4.7: Logarithmic plot of surface tension (mN/m) versus surfactant concentration (wt%) after the first extraction.

Table 4.5: Values of ST at the plateau, CMC, surface concentration and area per molecule for the surfactants after calculation of expected surfactant concentrations.

Property	PG3C10_2:1a_E1	PG3C10_2:1b_E1	PG3C10_10:1_E1
ST (mN/m) at the plateau	26.3	25.8	25.6
CMC (mmol/L)	2.7	3.7	2.3
Γ (µmol/m^2) from Langmuir isotherm	4.7	4.7	5.1
A (Å^2) from Langmuir isotherm	35.0	35.5	32.4
Γ (µmol/m^2) from Gibbs isotherm	3.9	3.9	4.5
A (Å^2) from Gibbs isotherm	42.4	42.6	37.3

PG3C10_10:1_E1 had the lowest area per molecule and the highest surface excess

concentration. This could be due to the higher fraction of monoesters. Monoesters have one head and one tail, which makes them likely to pack better. They also have a higher HLB value compared to diesters and triesters. These factors tighten the packing at the interface and result in a smaller area per molecule. Consequently, this leads to a higher number of molecules being adsorbed per unit area, thereby increasing the surface excess concentration. PG3C10_10:1_E1 also had the lowest surface tension, which could be a consequence of denser packing at the interface. The CMCs of the three batches were similar. This could mean that the fraction of monoesters did not significantly affect the CMC. However, it would be expected that the CMC of PG3C10_10:1_E1 would be the highest (monoesters are more hydrophilic than di- and triesters), which was not the case. The reason for this unusual trend is unclear. Steric hindrance in di- and triesters could result in an increase in the area per molecule, leading to looser packing and lower surface excess concentrations. This was seen in the cases of PG3C10_2:1a_E1 and PG3C10_2:1b_E1.

Table 4.6: CMC values for the surfactants after the first extraction.

Property	PG3C10_2:1a_E1	PG3C10_2:1b_E1	PG3C10_10:1_E1
CMC (mmol/L)	4.3	5.9	3.7

4.1.5 Clouding phenomena

Clouding was observed in the three surfactant batches at room temperature. For PG3C10_2:1a and PG3C10_2:1b, clouding increased with an increase in surfactant concentration. The solutions of PG3C10_2:1a_E1 and PG3C10_2:1b_E1 remained cloudy (after extraction). The clouding behaviors of PG3C10_10:1 and PG3C10_10:1_E1 are discussed in Section 4.1.5.2.

4.1.5.1 Cloud point measurements

Table 4.7 summarizes the results of cloud point tests performed using 1 wt% surfactant solutions. All solutions, except for PG3C10_10:1_E1 were cloudy at room temperature (before heating). No phase separation was observed for any of the batches upon cooling from 85 °C back to room temperature. The surfactant mixtures were also cooled from room temperature to 4 °C to study the effect of reduced temperature on clouding. The temperatures at which changes were observed in PG3C10_2:1a (70 °C and 85 °C) reduced to 40 °C and 56 °C in PG3C10_2:1a_E1 (after extraction). This could mean that the presence of excess polyglycerol in the surfactant mixture raises the cloud point of the solution. However, this has not been confirmed.

4.1.5.2 Clouding behavior of PG3C10_10:1

PG3C10_10:1 exhibited peculiar behavior with regard to clouding. Its 1 wt% solution was cloudy at room temperature, whereas the solutions of lower and higher concentrations were transparent (Figure 4.8 (a)). After placing the stock

solutions at 4 °C for 24 hours, the 1 wt% solution turned transparent, as shown in Figure 4.8 (b). When the solutions were allowed to return to room temperature from 4 °C, they all remained transparent. This means that the temperature history is relevant to clouding.

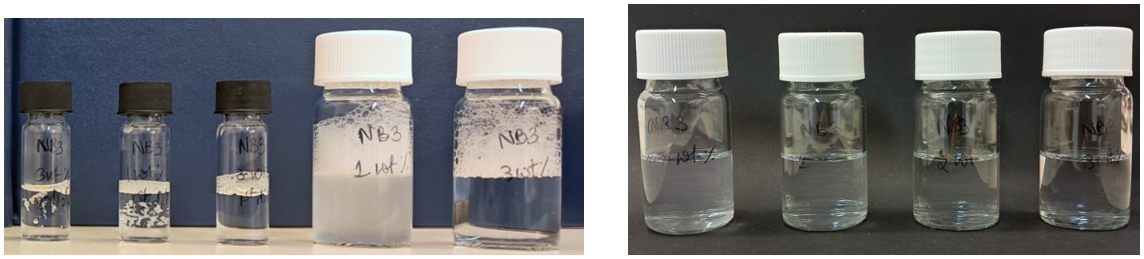

(a) **(b)**

Figure 4.8: Clouding observed in PG3C10_10:1: (a) at room temperature immediately after solution preparation (from left to right: 0.03 wt%, 0.1 wt%, 0.3 wt%, 1 wt%, 3 wt%), (b) stock solutions when kept at 4 °C for 24 hours after solution preparation (from left to right: 0.7 wt%, 1 wt%, 2 wt%, 3 wt%).

Table 4.7: Results of cloud point measurements for the surfactants synthesized through the solvent-free route.

Surfactant batch	Upon heating up to 85 °C	Upon cooling back to room temperature	Upon cooling to 4 °C
PG3C10_2:1a	Turned cloudier at 58 °C	Reversible	No change
PG3C10_2:1a_E1	No change	No change	Precipitated at 3 wt%
PG3C10_2:1b	Turned less cloudy at 70 °C, and then cloudier at 85 °C	Reversible	No change
PG3C10_2:1b_E1	Turned less cloudy at 40 °C, and then cloudier at 56 °C	Reversible	No change
PG3C10_10:1	Turned transparent at 66 °C	Reversible	Turned transparent
PG3C10_10:1_E1	No change	No change	No change

From Table 4.7, the 1 wt% solution of PG3C10_10:1 showed a different clouding behavior upon heating. It turned transparent upon heating and returned to being cloudy when cooled to room temperature. Due to this unusual behavior, along with the observations from Figure 4.8(a), two additional cloud point measurements were performed at 0.7 wt% and 2 wt%. The 0.7 wt% solution was transparent at room temperature and remained transparent upon heating up to 85 °C. No

clouding was observed. The 2 wt% solution was also transparent at room temperature, but started clouding at around 53 °C upon heating. It became the most cloudy at around 59 °C and remained that way even at higher temperatures. While cooling, it started becoming transparent at around 55 °C and turned fully transparent at around 46 °C. However, the reason for this behavior is still unknown and needs to be investigated further. The results of these cloud point measurements are illustrated in Figure 4.9, which is a plot of temperature against surfactant concentration. The shaded region is indicative of a narrow temperature and concentration range in which the PG3C10_10:1 solutions are cloudy.

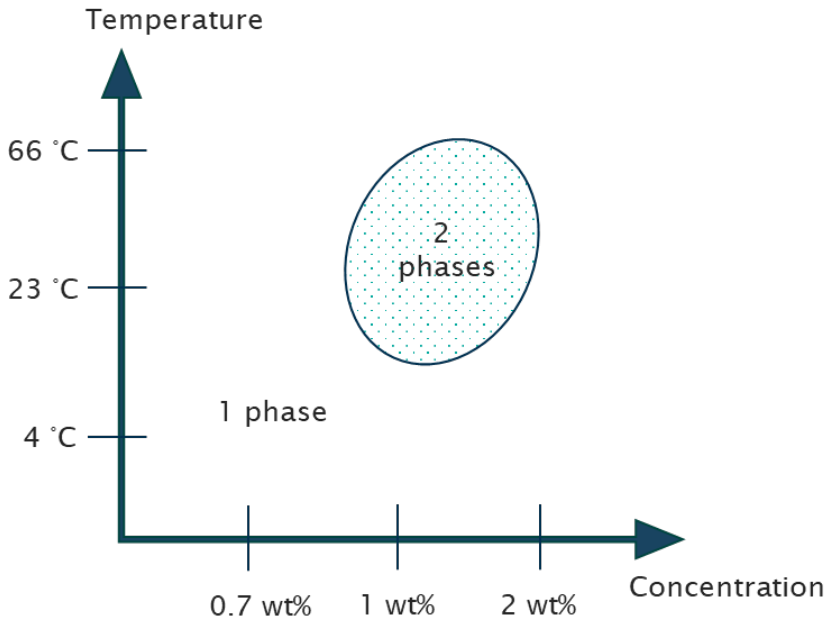

Figure 4.9: Plot of temperature (°C) against surfactant concentration (wt%) for PG3C10_10:1 solutions.

PG3C10_10:1_E1 exhibted clouding behavior at higher concentrations, i.e., at 2 wt% and 3 wt% (Figure 4.10 (a)). This was less intense compared to the clouding behavior of PG3C10_10:1. This shift in clouding to higher concentrations could be due to the removal of unreacted polyglycerol from the system, thereby altering the surfactant concentrations.

As mentioned earlier in Section 4.1.4, the expected fraction of surfactant in PG3C10_10:1 was 0.15. For a 1 wt% solution, the expected surfactant concentration would be 0.15 wt%. In Figure 4.8 (a), the 1 wt% solution of the unpurified surfactant is cloudy. So, theoretically, the concentration at which PG3C10_10:1_E1 would be expected to be cloudy (if it were 100% pure) is 0.15 wt%. To understand the shift in clouding upon purification, a 0.15 wt% solution of PG3C10_10:1_E1 was prepared to correspond to the expected surfactant concentration for a pure surfactant. Then, polyglycerol-3 was added until the concentration reached 1 wt% of PG3C10_10:1, i.e., the concentration at which the

unpurified surfactant was cloudy. This was done to determine whether the addition of polyglycerol-3 would reinduce clouding in the solutions. Clouding was not reinduced, which could be due to chemical changes that may have occurred in the polyglycerol molecules during synthesis, i.e., they could have reacted with some fatty acid molecules, which cannot be replaced with pure polyglycerol-3. However, this has not been confirmed.

The PG3C10_10:1_E1 stock solutions were placed at 4 °C for 48 hours, and they did not exhibit any visible changes, as can be seen in Figure 4.10 (b).

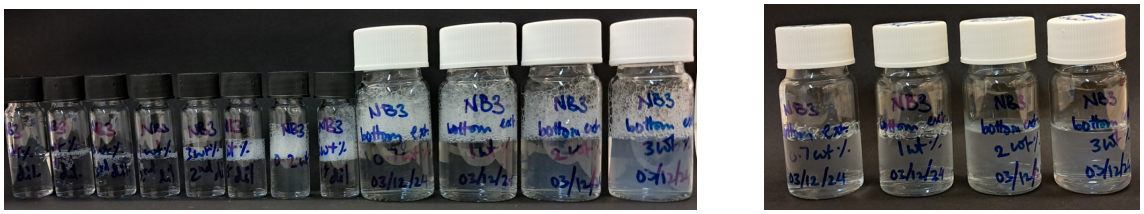

(a) **(b)**

Figure 4.10: Clouding observed in PG3C10_10:1_E1: (a) at room temperature with concentrations (in ascending order from left to right) listed in Table A.x immediately after solution preparation, (b) stock solutions when kept at 4 °C for 48 hours after solution preparation (from left to right: 0.7 wt%, 1 wt%, 2 wt%, 3 wt%).

4.1.5.3 Effect of salt addition on solubility

Table 4.8 summarizes the results of salt addition to 1 wt% surfactant solutions. In some cases, the salts enabled the solubilization of the surfactants at concentrations less than 1 wt%. The concentrations and ionic strengths at which solubilization occurred are specified in the table. The addition of NaF and NaSCN had no visible effect on the solubility of PG3C10_2:1a and PG3C10_2:1b. However, PG3C10_10:1 became cloudier with the addition of NaF (at 0.04 M) and solubilized with the addition of NaSCN at a high ionic strength, above 0.1 M. This could mean that salt addition affects the solubility of surfactants that contain more monoesters. However, PG3C10_10:1 has a much greater content of unreacted polyglycerol-3 than the other two surfactant batches, which could also cause the solubility changes to be more visible. The exact reasons for these results are still unknown, and further research needs to be performed.

Table 4.8: Effect of NaF and NaSCN addition on the solubility of PGEs synthesized through the solvent route.

Surfactant batch	Addition of NaF	Addition of NaSCN
PG3C10_2:1a	No visible effect	No visible effect
PG3C10_2:1b	No visible effect	No visible effect
PG3C10_10:1	Became less soluble at 0.04 M (0.95 wt%)	Solubilized above 0.1 M

4.1.6 Performance of the PGEs in cleaning applications

The PG3C10_2:1a, PG3C10_2:1b and PG3C10_10:1 formulations performed poorly in the cleaning tests. This could be due to the unreacted polyglycerol present in the surfactant mixtures, since they are unpurified. However, the PG3C10_10:1 formulation showed interesting behavior during contact angle measurements. Figure 4.11 is the plot of contact angle against time for the three formulations, and their contact angles measured after 60 seconds are listed in Table 4.9. The curves for the PG3C10_2:1a and PG3C10_2:1b formulations displayed similar behavior, and had the same contact angle after 60 seconds of measurement. Their slopes were steeper and they reached a plateau value quickly, which means that they adsorbed onto the solid surface quicker. However, the PG3C10_10:1 formulation had a considerably low contact angle. This could be due to greater monoester content or due to a higher amount of unreacted polyglycerol present in the surfactant mixture. The polyglycerol may have acted as an effective wetting agent on the soil, lowering the contact angle. However, this remains unclear. Further research needs to be done in this regard, along with cleaning tests using purified surfactants.

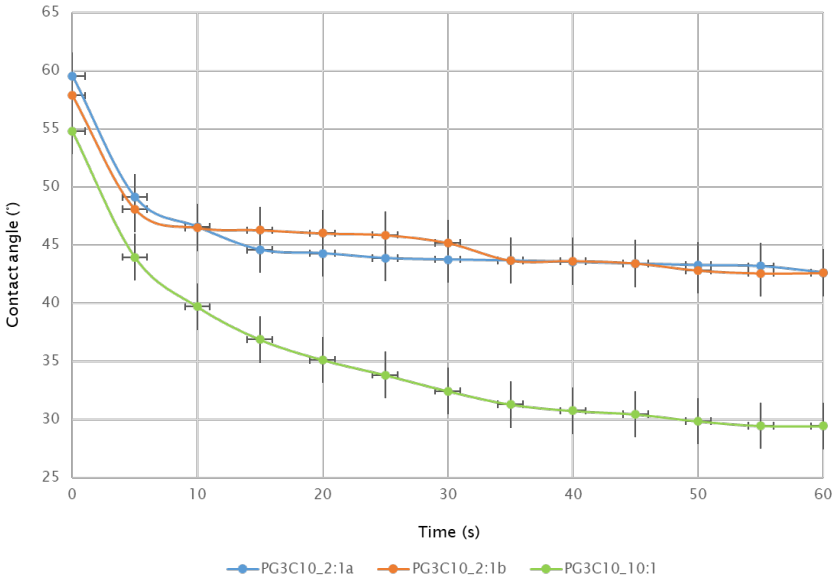

Figure 4.11: Plot of contact angle (°) against time (s) for PG3C10_2:1a, PG3C10_2:1b and PG3C10_10:1 formulations.

Table 4.9: Contact angles of PG3C10_2:1a, PG3C10_2:1b and PG3C10_10:1 formulations measured after 60 seconds.

Surfactant batch	Contact angle
PG3C10_2:1a	42.6°
PG3C10_2:1b	42.6°
PG3C10_10:1	29.4°

4.2 Surfactants synthesized through the solvent route

In order to broaden the scope of the work with more types of polyglycerols and chains, five surfactants were synthesized in solvent, all of which were colorless. The viscosity decreased with an increase in head group size, and increased with an increase in tail length. Their purities (Table 4.10) were assessed using their ^{1}H NMR spectra. The areas of the desired peaks were divided by the total peak area (excluding solvent peaks) to obtain the purity in percentage. The ^{1}H NMR spectra along with the integral values are depicted in Figures A.10, A.12, A.14, A.16 and A.18 in Section A.7.

Table 4.10: Purities of the surfactants synthesized in solvent.

Surfactant	Purity
PG3C10	86.6%
PG4C10	92.6%
PG6C10	94.1%
PG3C12	96.9%
PG3C14	95.5%

4.2.1 Surfactant composition analysis using LC-MS

The compositions of the surfactants were analyzed using LC-MS. It was not possible to perform a quantitative analysis as no reference standards were available. The Extracted Ion Chromatogram (EIC) areas of targeted compounds were grouped into compound types of interest and then compared (Figure 4.12) under the assumption that the ionization efficiencies of the compounds in each sample would be similar. Although this did not provide any insights into the absolute composition of the samples, it showed interesting trends in the relative composition. These were normalized to the highest combined EIC-area. The y-axis representing the area under the peak is often normalized to 100% to facilitate comparison and quantification of relative ion intensities. 2 µL injections of 10 ppm solutions were used, and it was expected that all samples would have a relative EIC area of 100%. The fact that they varied by an order of magnitude indicated that there were undetected compounds in some surfactant samples. This could be, for example, water or some other compounds that do not ionize well in the Electrospray Ionization (ESI) source. There could also be other compounds present in the surfactants that were not targeted in this analysis.

Figure 4.13 illustrates the ester composition of each surfactant. They are represented as the sums of the EIC areas for each of the target compounds. These were normalized to the sums of the areas for all compounds in each sample. The data for polyglycerol was not considered in Figure 4.13. This was done to compare the percentages of mono-, di-, and triesters. This was also not quantitative, but it

provided an idea of the ester composition. A greater amount of monoesters was present in the relatively hydrophilic surfactants, namely, PG3C10, PG4C10 and PG6C10. The more hydrophobic surfactants, PG3C12 and PG3C14, consisted predominantly of diesters. It could be that during synthesis, during the dropwise addition of acyl chloride, the longer fatty acid chains (C12 and C14) are more likely to react with an already formed ester due to stronger hydrophobic interactions between the tails (hydrophobic interactions are stronger compared to shorter fatty acid chains), leading to the formation of diesters rather than monoesters. However, this hypothesis has not been confirmed. Another conclusion that can be drawn from these results is that the synthesis of relatively hydrophilic surfactants may be preferred if a greater percentage of monoesters is desired.

Traces of decanoic acid were detected in PG3C10. Decanoic acid is surface active and could potentially affect the surface properties of the surfactant.

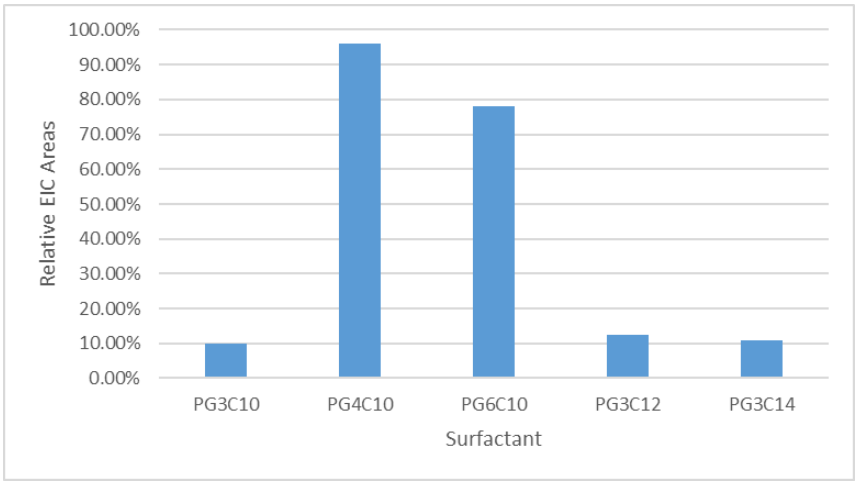

Figure 4.12: Relative EIC areas among the surfactants synthesized in solvent.

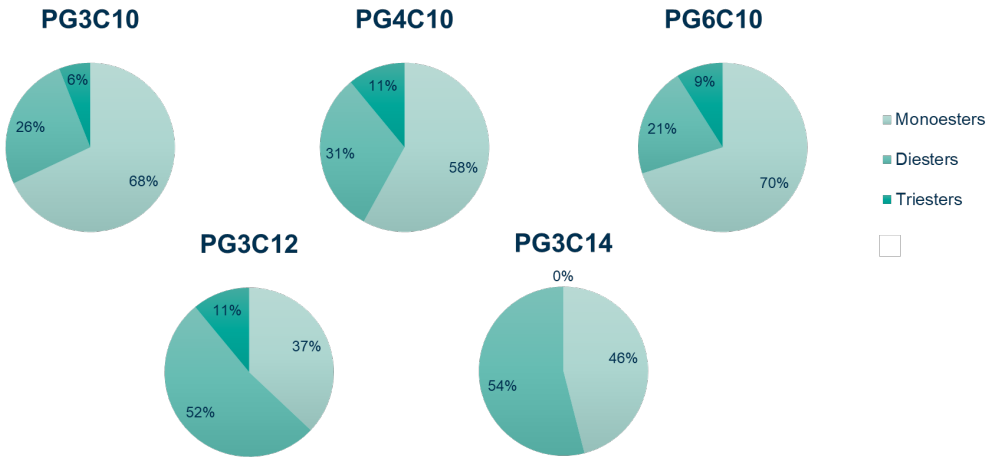

Figure 4.13: Normalized ester compositions after the exclusion of polyglycerol content.

4.2.2 Qualitative and quantitative analysis using IR and NMR spectroscopy

IR spectroscopy was performed for the five surfactants. An intense peak was found at 1735 − 1740 cm^1 (carbonyl group) for all surfactants, which confirmed the presence of esters. The IR spectra are shown in Figure A.9 in Section A.6.

NMR spectroscopy was performed for quantitative analysis. Upon analysis of the spectra with respect to the chemical shifts of the peaks, it was concluded that the desired PGEs were formed during synthesis. The ^{1}H NMR and ^{13}C NMR spectra for the surfactants are given in Section A.7, along with details of the peak positions and integrals.

4.2.3 Effect of varying head group size on surface properties

ST curves were plotted for PG3C10, PG4C10 and PG6C10 to compare surface properties based on varying head group size. The curves are shown in Figure 4.14. The values of ST at the plateau, CMC, surface excess concentration, and area per molecule are given in Table 4.11. The surfactant concentrations on the x-axis were corrected according to the calculated purities from ^{1}H NMR (Table 4.10). A dip was observed near the CMC in the ST curve for PG3C10. This could be due to hydrophobic surface-active impurities present in the surfactant, which could be decanoic acid. It could also be explained by the relatively low purity of PG3C10, as a dip was not observed in the ST curves of the other surfactants.

Surface tension typically increases with an increase in surfactant hydrophilicity. However, from Table 4.11, the surface tensions of the surfactants were similar regardless of the size of the head group, i.e., they all had the same surface activity, which was unexpected. The surfactants had low surface tensions in general, indicating good surface activity. The trend for the CMC is difficult to interpret due to the purity and complexity of these systems. Typically, CMC increases with an increase in surfactant hydrophilicity, which means that PG6C10 would be expected to have the highest CMC due to a larger head group size and more repulsion between molecules at the interface. However, this was not observed. It is also difficult to interpret this result due to the chemical complexity of polyglycerol-6. The analysis of the surface excess concentrations and the areas per molecule was carried out using the data obtained from the Gibbs isotherm. PG3C10 had the highest surface excess concentration and the lowest area per molecule, meaning that it packed better at the interface. This could be due to its smaller head group, which allows for less repulsion.

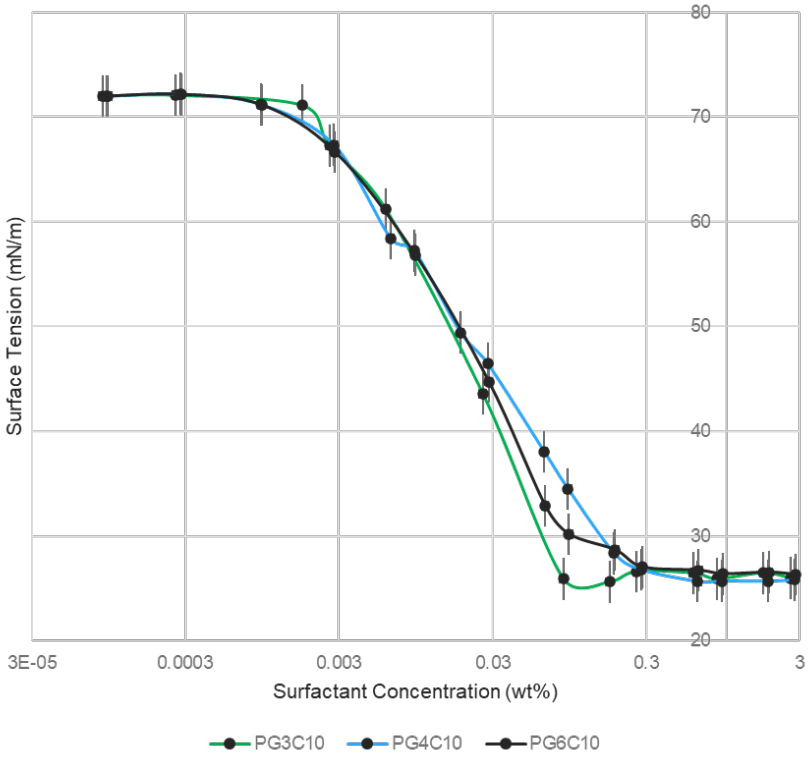

Figure 4.14: Logarithmic plot of surface tension (mN/m) versus surfactant concentration (wt%) for PG3C10, PG4C10 and PG6C10.

Table 4.11: Values of ST at the plateau, CMC, surface concentration and area per molecule for PG3C10, PG4C10 and PG6C10.

Property	PG3C10	PG4C10	PG6C10
ST (mN/m) at the plateau	26.3	25.7	26.4
CMC (mmol/L)	2.2	5.0	2.0
Γ (µmol/m^2) from Langmuir isotherm	11.1	4.8	6.7
A (Å^2) from Langmuir isotherm	15.0	34.5	24.9
Γ (µmol/m^2) from Gibbs isotherm	5.3	3.9	4.8
A (Å^2) from Gibbs isotherm	31.1	42.9	34.6

4.2.4 Effect of varying tail length on surface properties

Adsorption isotherms were measured for PG3C10, PG3C12 and PG3C14 to compare surface properties based on varying tail length. The curves are shown in Figure 4.15. The values of ST at the plateau, CMC, surface excess concentration, and area per molecule are given in Table 4.12. The surfactant concentrations on the x-axis were corrected according to the calculated purities from ^{1}H NMR (Table 4.10).

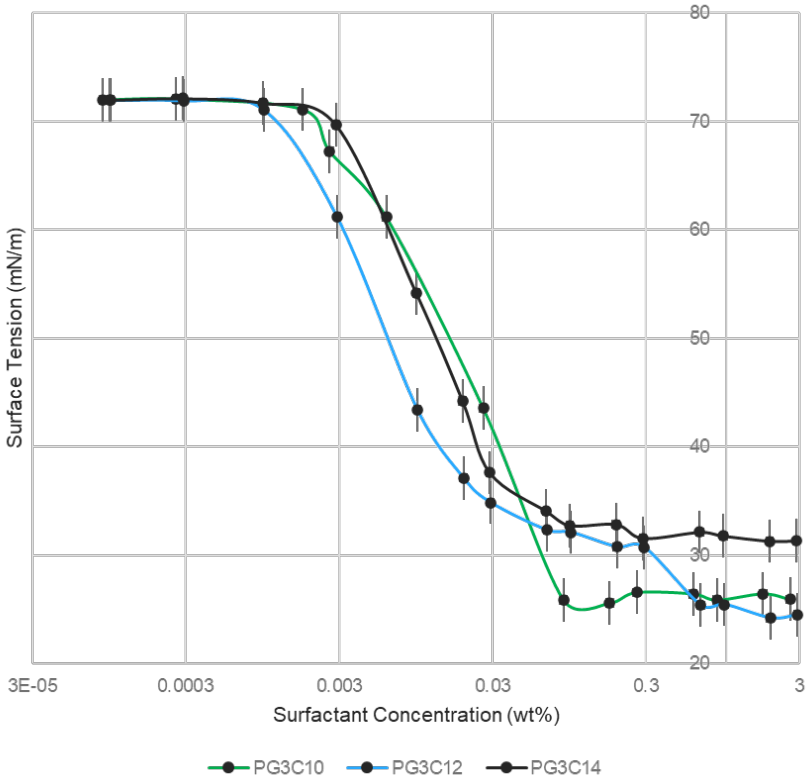

Figure 4.15: Logarithmic plot of surface tension (mN/m) versus surfactant concentration (wt%) for PG3C10, PG4C10 and PG6C10.

Table 4.12: Values of ST at the plateau, CMC, surface concentration and area per molecule for PG3C10, PG3C12 and PG3C14.

Property	PG3C10	PG3C12	PG3C14
ST (mN/m) at the plateau	26.3	24.7	32.0
CMC (mmol/L)	2.2	0.7	1.1
Γ (µmol/m^2) from Langmuir isotherm	11.1	8.6	27.5
A (Å^2) from Langmuir isotherm	15.0	19.4	6.0
Γ (µmol/m^2) from Gibbs isotherm	5.3	6.0	5.8
A (Å^2) from Gibbs isotherm	31.1	27.8	28.7

Surface tension typically decreases with an increase in surfactant hydrophobicity. From Table 4.12, PG3C10 and PG3C12 exhibited this behavior, but the surface tension of PG3C14 was higher than that of PG3C12. This was unexpected. CMC typically decreases with an increase in surfactant hydrophobicity. However, the CMC of PG3C14 was higher than that of PG3C12. The analysis of the surface excess concentrations and the areas per molecule were carried out using the data obtained from the Gibbs isotherm. PG3C12 had the highest surface excess concentration and the lowest area per molecule, meaning better packing at the interface. It would be expected that the packing would be best for PG3C14 due to its longer tail length and greater hydrophobic interactions at the interface, but this was not observed.

The deviation of PG3C14 from expected trends could be attributed to its poor solubility in water. Another interesting observation was the shape of the PG3C12 curve, where two plateaus are present. This could be due to the cloudiness of the surfactant solution and the complex nature of micellization.

4.2.5 Clouding phenomena

Clouding phenomena were observed in the five surfactants at different concentrations of their solutions. The cloudiness of 1 wt% surfactant solutions increased in the following order: PG6C10, PG4C10, PG3C10, PG3C12, PG3C14. This followed the expected trend, with cloudiness increasing with an increase in hydrophobicity.

4.2.5.1 Cloud point measurements

Table 4.13 summarizes the results of cloud point tests performed using 1 wt% surfactant solutions. The surfactants are listed from top to bottom in increasing order of cloudiness at room temperature (before heating). PG6C10 turned cloudier upon heating, while the other surfactants turned less cloudy. Typically, the cloud point increases with an increase in hydrophilicity. However, in the case of PG3C10, PG4C10 and PG6C10, the cloud point increased with a decrease in the head group size (or a decrease in hydrophilicity). This could be due to impurities or due to the complex nature of polyglycerol-6, which contains various structures like linear (with varying glycerol units), branched and cyclic structures. This could have led to a deviation from expected behavior. The expected trend was exhibited by PG3C10, PG3C12 and PG3C14, where the cloud point decreased with an increase in hydrophobicity. Phase separation was observed for all surfactants while cooling from 85 °C to room temperature.

Table 4.13: Results of cloud point measurements for the surfactants synthesized through the solvent route.

Surfactant	Upon heating up to 85 °C	Cloud point (°C)	Upon cooling back to room temperature
PG6C10	Turned cloudier	45	Phase separation
PG4C10	Turned less cloudy	51	Phase separation
PG3C10	Turned less cloudy	53	Phase separation
PG3C12	Turned less cloudy	46	Phase separation
PG3C14	Turned less cloudy	35	Phase separation

4.2.5.2 Effect of salt addition on solubility

Table 4.14 summarizes the results of salt addition to 1 wt% surfactant solutions. In some cases, the salts solubilized the surfactants at concentrations less than 1 wt%. The concentrations and ionic strengths at which solubilization occurred are specified in the table. The surfactants are listed from top to bottom in increasing

order of cloudiness. The PG6C10 solution became cloudier with the addition of NaF and solubilized with the addition of NaSCN at an ionic strength of 0.04 M. This could be due to the fact that the PG6C10 solution was less cloudy prior to salt addition, which made it easier to visually observe changes in solubility. No changes were observed for PG4C10 upon the addition of NaSCN, which was unusual since PG3C10 (which was cloudier than PG4C10) was solubilized at a high ionic strength of 0.42 M and a low surfactant concentration of 0.17 wt%. This strange behavior could be due to the presence of impurities in the surfactants. NaSCN could interact with these impurities in PG3C10, making it appear soluble. However, this has not been confirmed, and the mechanism of interactions between the salt and the impurities is unknown. The addition of NaF and NaSCN did not have a visible effect on PG3C12 and PG3C14. This could be due to the poor solubility of these surfactants in water.

Table 4.14: Effect of NaF and NaSCN addition on the solubility of PGEs synthesized through the solvent route.

Surfactant	Addition of NaF	Addition of NaSCN
PG6C10	Became less soluble	Solubilized at 0.04 M (0.95 wt%)
PG4C10	No visible effect	No visible effect
PG3C10	No visible effect	Solubilized at 0.42 M (0.17 wt%)
PG3C12	No visible effect	No visible effect
PG3C14	No visible effect	No visible effect

4.2.5.3 Alkaline hydrolysis of PGEs using NaOH

No change in the solubility of PG3C10 was observed in the 7 vials after 24 hours at 60 °C. The temperature was increased to 70 °C to increase the rate of reaction and promote hydrolysis. After 24 hours, changes were observed in some vials. These are shown in Figure 4.16. It was observed that the solubility of PG3C10 improved at certain molar ratios. The molar ratios corresponding to each vial are given in Table 3.4. The solubility of the surfactant improved in vials 5 and 6, whose molar ratios of NaOH to PG3C10 were 3 and 3.5, respectively. This could be due to the formation of water-soluble sodium caprate (sodium salt of decanoic acid) upon hydrolysis. The hydrolysis is unimer driven. The increase in temperature to 70 °C resulted in an increase in reaction rate, but could have disrupted the micelles, resulting in an increase in unimers. Unimers hydrolyze more readily than micelles because the negative head groups of micelles repel hydroxyl ions. Thus, a disruption of micelles at a higher temperature could have led to increased solubility of the surfactants.

The solubility decreased in vial 7, whose molar ratio of NaOH to PG3C10 was 4. This could be due to the common ion effect, which occurs at higher concentrations of NaOH. This effect is based on the fact that sodium caprate and NaOH have a common ion (Na^+), which leads to salt precipitation, resulting in a decrease in solubility as a consequence of a salt effect.

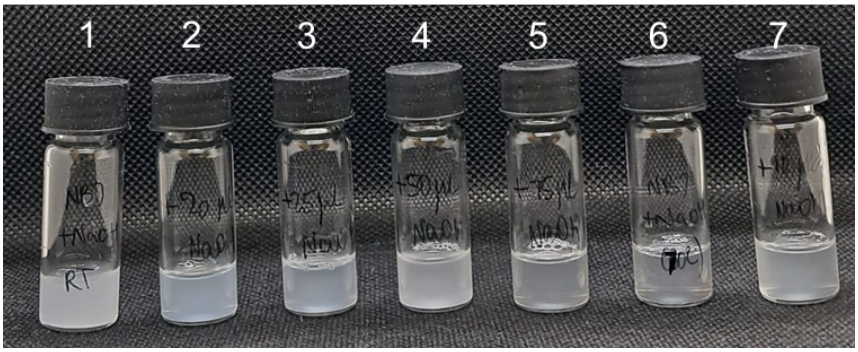

Figure 4.16: Vials of 1 wt% PG3C10 solutions (details given in Table 3.4) after 24 hours at 70 °C.

4.2.6 Performance of the PGEs in cleaning applications

Figure 4.17 shows the comparison of the cleaning performances of PG3C10, PG4C10 and PG6C10 formulations on a soiled ceramic plate. It was observed that the PG6C10 formulation picked up the soil off the surface more effectively, but had lower wettability than the other two formulations. This is due to the greater hydrophilicity of PG6C10. The PG3C10 formulation had the lowest cleaning efficiency and the highest wettability (PG3C10 is more hydrophobic). The formulations of PG3C12 and PG3C14 performed poorly in the cleaning tests. This could be attributed to the poor solubility of these surfactants in water. The PG3C14 formulation remained cloudy even after the addition of a significant amount of SXS.

Figure 4.17: Cleaning performances of PG3C10, PG4C10 and PG6C10 (from left to right) formulations on a soiled ceramic plate.

Figure 4.18 shows the plot of contact angle against time for the five formulations. The contact angles measured after 60 seconds are listed in Table 4.15. Contact angle (when measured on a hydrophobic surface such as paraffin wax) typically increases with an increase in surfactant hydrophilicity. However, while comparing the PG3C10, PG4C10 and PG6C10 formulations, it was observed that PG6C10

had a slightly lower contact angle than PG4C10. This could be due to SXS, but this has not been confirmed. While comparing the PG3C10, PG3C12 and PG3C14 formulations, it was observed that PG3C14 had a much higher contact angle than PG3C12, while it was expected to provide a better wettability. This could be due to the solubility issues of PG3C14. The slopes of the curves is a proxy of time required for the surfactants to adsorb onto the solid surface. PG3C10 adsorbed the quickest, since the slope was steeper and the curve took more time to reach a plateau value. This could be attributed to its relatively small molecular size. PG3C14 took the longest time to adsorb, which could be attributed to its poor solubility.

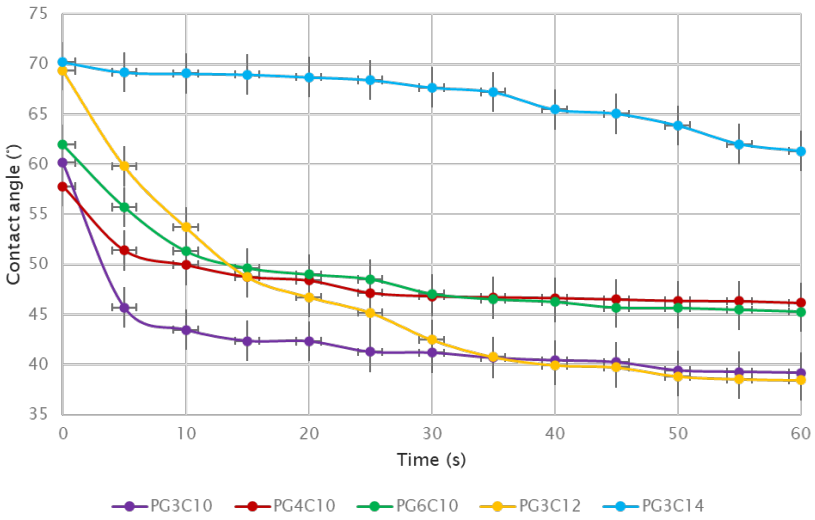

Figure 4.18: Plot of contact angle (°) against time (s) for PG3C10, PG4C10, PG6C10, PG3C12 and PG3C14 formulations.

Table 4.15: Contact angles of PG3C10, PG4C10, PG6C10, PG3C12 and PG3C14 formulations measured after 60 seconds.

Surfactant	Contact angle
PG3C10	39.2°
PG4C10	46.2°
PG6C10	45.3°
PG3C12	38.5°
PG3C14	61.3°

The PG6C10 formulation was concluded to be better at cleaning than the other two. Thus, its performance compared with a similar formulation of a commercial PEG-based surfactant called Berol O_X 91-6. Berol O_X 91-6 contains hydrophobic tails ranging from 9 to 11 carbons long. It is more hydrophobic than PG6C10. Its head group has a broad distribution of ethylene oxide molecules, which makes it a suitable and practical comparison to PG6C10, where the polyglycerol-6 head group

is also complex in nature. The molecule in Figure 4.19 shows the surfactant structure, with 10 carbons in the tail and 6 ethylene oxide units in the head group. This was meant for ease of comparison to PG6C10.

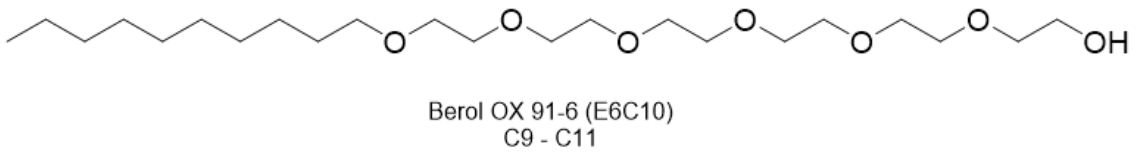

Figure 4.19: Chemical structure of Berol O_X 91-6.

Figure 4.20 shows the cleaning performance of PG6C10 and Berol O_X 91-6 formulations. The PG6C10 formulation cleaned better in terms of picking the soil off the surface, but the Berol O_X 91-6 formulation cleaned better in terms of wettability, i.e., it had greater wettability. Figure 4.21 is the plot of their contact angles against time, and their contact angles measured after 60 seconds are given in Table 4.16.

Figure 4.20: Cleaning performances of PG6C10 (left) and Berol O_X 91-6 (right) formulations on a soiled ceramic plate.

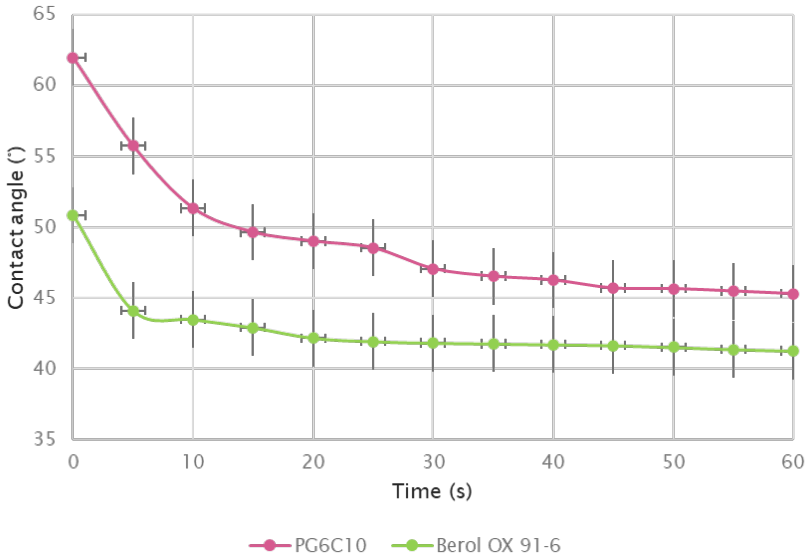

Figure 4.21: Plot of contact angle (°) against time (s) for PG6C10 and Berol O_X 91-6 formulations.

Table 4.16: Contact angles of PG6C10 and Berol O_X 91-6 formulations measured after 60 seconds.

Surfactant	Contact angle
PG6C10	45.3°
Berol O_X 91-6	41.3°

From Figure 4.21, the PG6C10 formulation took more time to adsorb on the solid surface, since the curve reached a plateau value later. It also had a higher contact angle (Table 4.16) than the Berol O_X 91-6 formulation, which explains the better wettability of the latter. Overall, the cleaning efficiency of the two were similar, and some adjustments to the PG6C10 formulation could enhance performance. These results suggest that PGEs are promising alternatives to fossil-based surfactants in cleaning applications.

The contact angles of the PGE formulations reduced further when measured beyond 60 seconds, which could mean that PGEs take a longer time to adsorb onto solid surfaces compared to PEG-based surfactants, like Berol O_X 91-6, which usually adsorb quickly (the plateau value of contact angle remained stable after a relatively short period of time). This indicates that PGEs could possibly clean better if kept on the surface for a longer period of time. This would be of interest for future research in this area.

5
Conclusion

PG3C10 surfactant was synthesized using different reaction conditions through the solvent-free route. PG3C10_2:1a and PG3C10_2:1b, which were synthesized using a polyglycerol-to-fatty acid molar ratio of 2, contained approximately 53% and 48% monoesters, respectively. PG3C10_10:1, which was synthesized using a molar ratio of 10, contained around 68% monoesters after the first extraction. This indicates that a higher polyglycerol-to-fatty acid molar ratio promotes monoester formation, as expected. The pendant drop tensiometry results showed a low surface tension at the plateau for all surfactants, indicating good surface activity. PG3C10_10:1 had the lowest area per molecule and the highest surface excess concentration. This could be due to the higher fraction of monoesters, resulting in denser packing at the interface.

It is still unclear whether one-phase synthesis results in a higher monoester content than two-phase synthesis due to the lack of quantitative data. However, from the normalized data of the ester composition, it appears that more monoesters are present in comparison to diesters and triesters.

PG3C10, PG4C10 and PG6C10 were found to have the same surface activity, regardless of the head group, which was unexpected. PG3C10 had the highest surface excess concentration and the lowest area per molecule, meaning that it packed better at the interface. During the investigation of the effect of tail length on surface properties, it was observed that PG3C14 deviated from expected trends. It was found to have higher CMC and surface tension than PG3C12. This could be attributed to solubility issues of the surfactant.

The PG6C10 formulation cleaned better in terms of picking the soil off the surface, while the Berol O_X 91-6 formulation had greater wettability. Overall, the two formulations had comparable performances, suggesting that PGEs are a promising alternative to fossil-based surfactants in cleaning applications.

Polyglycerol is chemically complex, which makes it challenging to fully understand the properties of PGEs. In order to investigate the structure-property relationship in these esters, obtaining pure monoesters and evaluating their properties are essential. Further investigation of clouding phenomena is important to gain a deeper understanding of the behavior of PGEs. Adsorption on solid surfaces could then be evaluated. It would also be of interest to modify the compositions of PGE formulations to enhance their cleaning efficacy.

Bibliography

1. Farias CBB, Almeida FC, Silva IA, Souza TC, Meira HM, Cássia F. Soares da Silva R de, Luna JM, Santos VA, Converti A, Banat IM, and Sarubbo LA. Production of green surfactants: Market prospects. *Electronic Journal of Biotechnology*. Vol. 51. 2021 :28–39
2. Damle S and Madankar C. An overview on eco-friendly polyglycerol esters of fatty acid, synthesis and applications. *Tenside Surfactants Detergents*. Vol. 60. 6. 2023 :611–21
3. Stanimirova RD, Danov KD, Georgiev MT, and Petkov JT. Colloid, interface, and foam properties of water-soluble polyglycerol esters solutions. *Journal of Colloid and Interface Science*. Vol. 677. 2025 :250–63
4. Márquez-Alvarez C, Sastre E, and Pérez-Pariente. Solid catalysts for the synthesis of fatty esters of glycerol, polyglycerols and sorbitol from renewable resources. *Topics in Catalysis*. Vol. 27. 2004 :105–17
5. Parasuraman S, Anish R, Balamurugan S, Muralidharan S, Kumar KJ, and Vijayan V. An Overview of Liquid Chromatography-Mass Spectroscopy Instrumentation. *Pharmaceutical methods*. Vol. 5. 2014 :47
6. Glassford SE, Byrne B, and Kazarian SG. Recent applications of ATR FTIR spectroscopy and imaging to proteins. *Biochimica et Biophysica Acta (BBA) - Proteins and Proteomics*. Vol. 1834. 12. 2013 :2849–58
7. Liu X, Yu Q, Song A, Dong S, and Hao J. Progress in nuclear magnetic resonance studies of surfactant systems. *Current Opinion in Colloid Interface Science*. Vol. 45. Surfactants. 2020 :14–27
8. Esfandiarian A, Maghsoudian A, Davarpanah A, Tamsilian Y, and Kord S. Developing a novel procedure in utilizing pendant drop method for determination of ultra-low interfacial tension and surface tension in near-miscibility conditions. *Journal of Petroleum Science and Engineering*. Vol. 215. 2022 :110607
9. Kronberg B, Holmberg K, and Lindman B. Types of Surfactants, their Synthesis, and Applications. *Surface Chemistry of Surfactants and Polymers*. John Wiley & Sons, Ltd, 2014. Chap. 1:1–47
10. Kronberg B, Holmberg K, and Lindman B. Surface and Interfacial Tension. *Surface Chemistry of Surfactants and Polymers*. John Wiley & Sons, Ltd, 2014. Chap. 12:231–49
11. Pan Z, Trusler J, Jin Z, and Zhang K. Interfacial property determination from dynamic pendant-drop characterizations. *Nature Protocols*. Vol. 20. 2025 :363–386

12. Kronberg B, Holmberg K, and Lindman B. Surfactant Self-Assembly: General Aspects and Spherical Micelles. *Surface Chemistry of Surfactants and Polymers*. John Wiley & Sons, Ltd, 2014. Chap. 4:75–94
13. Martínez-Balbuena L, Arteaga-Jiménez A, Hernández-Zapata E, and Márquez-Beltrán C. Applicability of the Gibbs Adsorption Isotherm to the analysis of experimental surface-tension data for ionic and nonionic surfactants. *Advances in Colloid and Interface Science*. Vol. 247. 2017 :178–84
14. Kronberg B, Holmberg K, and Lindman B. Surfactant Adsorption at Solid Surfaces. *Surface Chemistry of Surfactants and Polymers*. John Wiley & Sons, Ltd, 2014. Chap. 8:153–73
15. Ferri JK and Stebe KJ. Which surfactants reduce surface tension faster? A scaling argument for diffusion-controlled adsorption. *Advances in Colloid and Interface Science*. Vol. 85. 1. 2000 :61–97
16. Kalam S, Abu-Khamsin SA, Kamal MS, and Patil S. Surfactant Adsorption Isotherms: A Review. *ACS Omega*. Vol. 6. 48. 2021 :32342–8
17. Kronberg B, Holmberg K, and Lindman B. Wetting and Wetting Agents, Hydrophobization and Hydrophobizing Agents. *Surface Chemistry of Surfactants and Polymers*. John Wiley & Sons, Ltd, 2014. Chap. 20:377–90
18. Mukherjee P, Padhan SK, Dash S, Patel S, and Mishra BK. Clouding behaviour in surfactant systems. *Advances in Colloid and Interface Science*. Vol. 162. 1. 2011 :59–79
19. Lindman B, Medronho B, and Karlström G. Clouding of nonionic surfactants. *Current Opinion in Colloid Interface Science*. Vol. 22. 2016 :23–9
20. Kronberg B, Holmberg K, and Lindman B. Surfactants and Polymers Containing Oxyethylene Groups Show a Complex Behavior. *Surface Chemistry of Surfactants and Polymers*. John Wiley & Sons, Ltd, 2014. Chap. 7:137–52
21. Vera RE, Salazar-Rodríguez F, Marquez R, and Forgiarini AM. How the Influence of Different Salts on Interfacial Properties of Surfactant–Oil–Water Systems at Optimum Formulation Matches the Hofmeister Series Ranking. *Journal of Surfactants and Detergents*. Vol. 23. 3. 2020 :603–15
22. Kronberg B, Holmberg K, and Lindman B. Surfactant Self-Assembly: Beyond the Spherical Micelle. *Surface Chemistry of Surfactants and Polymers*. John Wiley & Sons, Ltd, 2014. Chap. 6:113–36
23. Uner A and Yilmaz F. Efficiency of Laundry Polymers Containing Liquid Detergents for Hard Surface Cleaning. *Journal of Surfactants and Detergents*. Vol. 18. 2. 2015 :213–24

A

Appendix 1

A.1 Reaction parameters for PGEs synthesized through the solvent-free route.

Table A.1: Reaction parameters for PGEs synthesized through the solvent-free route.

Batch	Amount of polyglycerol-3	Amount of decanoic acid	Molar ratio of polyglycerol-3 to decanoic acid	Amount of PTSA catalyst	Reaction temperature (°C)
1	41,8065 g (0.174 mol, 2 equiv)	14,9901 g (0.087 mol, 1 equiv)	2	0,1621 g (0.00085 mol, 0.098 equiv)	135
2	41.8433 g (0.174 mol, 2 equiv)	15.0644 g (0.0874 mol, 1 equiv)	2	0.1667 g (0.00088 mol, 0.01 equiv)	105
3	209.9 g (0.874 mol, 10.03 equiv)	15.0 g (0.0871 mol, 1 equiv)	10	0.1667 g (0.00088 mol, 0.01 equiv)	105

A.2 Logarithmic concentration series for surface tension measurements

Table A.2: Logarithmic concentration series for PG3C10_2:1a, PG3C10_2:1b, PG3C10_10:1 and polyglycerol-3.

PG3C10_2:1a	PG3C10_2:1b	PG3C10_10:1	Polyglycerol-3
3 wt%	3 wt%	3 wt%	3 wt%
2 wt%	2 wt%	2 wt%	1 wt%
1 wt%	1 wt%	1 wt%	0.3 wt%
0.7 wt%	0.7 wt%	0.7 wt%	0.1 wt%
0.3 wt%	0.3 wt%	0.3 wt%	0.03 wt%
0.2 wt%	0.2 wt%	0.2 wt%	0.01 wt%
0.1 wt%	0.1 wt%	0.1 wt%	0.003 wt%
0.07 wt%	0.03 wt%	0.03 wt%	0.001 wt%
0.03 wt%	0.01 wt%	0.01 wt%	0.0003 wt%
0.01 wt%	0.003 wt%	0.003 wt%	0.0001 wt%
0.003 wt%	0.001 wt%	0.001 wt%	
0.001 wt%	0.0003 wt%	0.0003 wt%	
0.0003 wt%	0.0001 wt%	0.0001 wt%	
0.0001 wt%			

Table A.3: Logarithmic concentration series for PG3C10_2:1a_E1, PG3C10_2:1b_E1, PG3C10_10:1_E1.

Concentrations of surfactant solutions
3 wt%
2 wt%
1 wt%
0.7 wt%
0.3 wt%
0.2 wt%
0.1 wt%
0.03 wt%
0.01 wt%
0.003 wt%
0.001 wt%
0.0003 wt%

Table A.4: Logarithmic concentration series for PG3C10, PG4C10, PG6C10, PG3C12 and PG3C14.

PG3C10	PG4C10	PG6C10	PG3C12	PG3C14
3 wt%	3 wt%	3 wt%	3 wt%	3 wt%
2 wt%	2 wt%	2 wt%	2 wt%	2 wt%
1 wt%	1 wt%	1 wt%	1 wt%	1 wt%
0.7 wt%	0.7 wt%	0.7 wt%	0.7 wt%	0.7 wt%
0.3 wt%	0.3 wt%	0.3 wt%	0.3 wt%	0.3 wt%
0.2 wt%	0.2 wt%	0.2 wt%	0.2 wt%	0.2 wt%
0.1 wt%	0.1 wt%	0.1 wt%	0.1 wt%	0.1 wt%
0.03 wt%	0.07 wt%	0.07 wt%	0.07 wt%	0.07 wt%
0.007 wt%	0.03 wt%	0.03 wt%	0.03 wt%	0.03 wt%
0.003 wt%	0.02 wt%	0.01 wt%	0.02 wt%	0.02 wt%
0.002 wt%	0.01 wt%	0.003 wt%	0.01 wt%	0.01 wt%
0.0003 wt%	0.007 wt%	0.001 wt%	0.003 wt%	0.003 wt%
0.0001 wt%	0.003 wt%	0.0003 wt%	0.001 wt%	0.001 wt%
	0.001 wt%	0.0001 wt%	0.0003 wt%	0.0003 wt%
	0.0003 wt%		0.0001 wt%	0.0001 wt%
	0.0001 wt%			

A.3 Titration curves for the PGEs synthesized through the solvent-free route

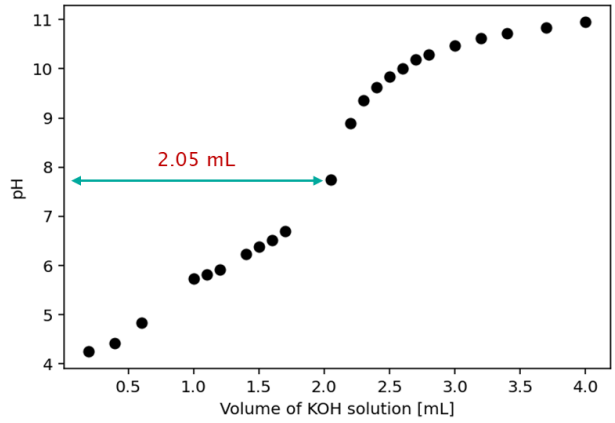

(a) PG3C10_2:1a

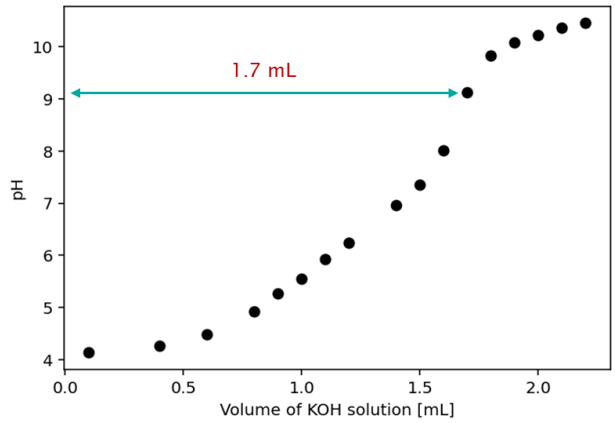

(b) PG3C10_2:1b

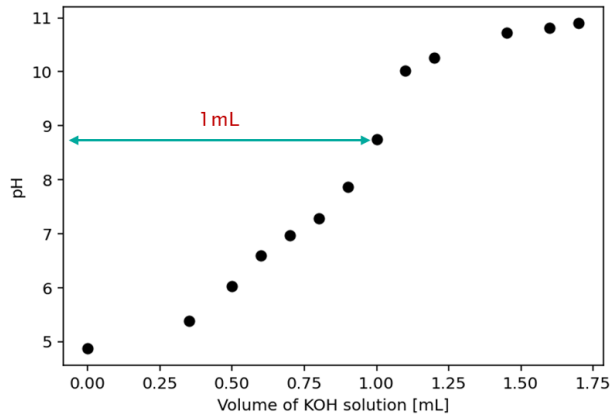

(c) PG3C10_10:1

Figure A.1: Titration curves of pH against volume of KOH solution for the surfactants synthesized through the solvent-free route.

A.4 NMR data and spectra for PGEs synthesized through the solvent-free route

Figure A.2 shows the comparison of the ^{1}H NMR spectra of PG3C10_2:1a (^{1}H NMR (600 MHz, MeOD) 4.31 – 3.43 (m, 31H), 2.38 (dq, J = 7.0, 3.5 Hz, 2H), 1.65 (t, J = 7.3 Hz, 2H), 1.41 – 1.28 (m, 13H), 0.93 (t, J = 6.9 Hz, 3H)) and PG3C10_2:1a_E1 (^{1}H NMR (600 MHz, MeOD) 4.32 – 3.42 (m, 18H), 2.37 (dq, J = 10.6, 7.7 Hz, 2H), 1.65 (q, J = 7.2 Hz, 2H), 1.41 – 1.27 (m, 13H), 0.94 (t, J = 6.9 Hz, 3H)).

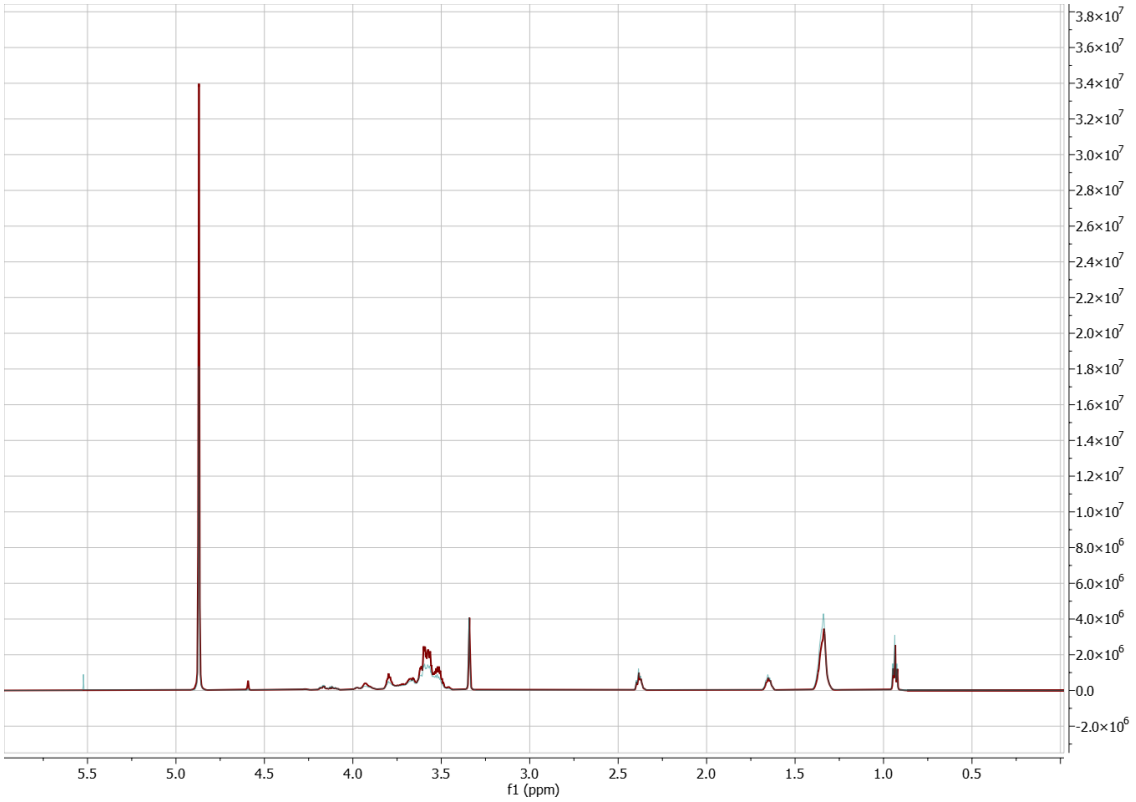

Figure A.2: Comparison of the ^{1}H NMR spectra of PG3C10_2:1a (red) and PG3C10_2:1a_E1 (blue).

Figure A.3 shows the comparison of the ^{13}C NMR spectra of PG3C10_2:1a (^{13}C NMR (151 MHz, MeOD) 81.81, 80.03, 72.48, 72.21, 71.35, 71.15, 70.85, 70.82, 69.67, 69.29, 68.17, 65.14, 62.92, 61.35, 61.15, 33.83, 33.55, 31.64, 29.18, 29.02, 28.81, 24.64, 22.33, 13.05) and PG3C10_2:1a_E1 (^{13}C NMR (151 MHz, MeOD) 174.05, 81.82, 80.05, 72.50, 72.21, 70.86, 70.82, 69.76, 69.28, 68.17, 65.13, 62.93, 61.36, 61.15, 60.41, 33.82, 33.55, 31.65, 29.18, 29.02, 28.81, 24.63, 22.33, 13.04).

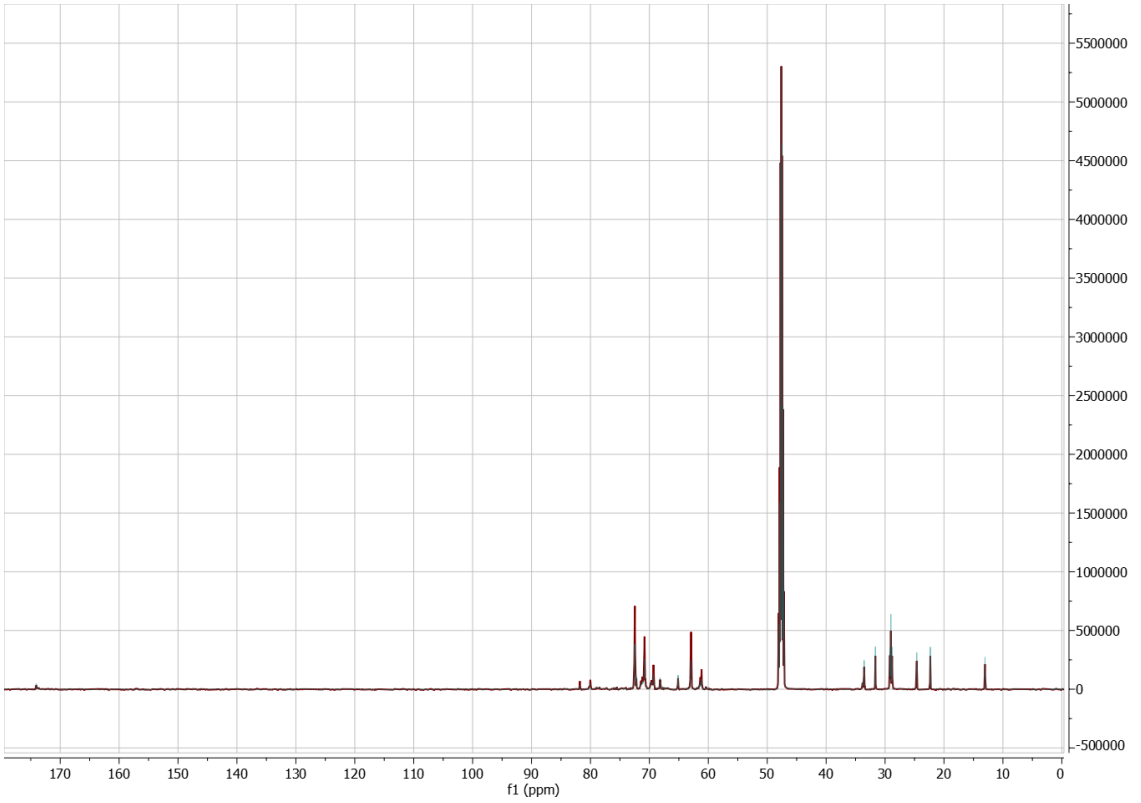

Figure A.3: Comparison of the ^{13}C NMR spectra of PG3C10_2:1a (red) and PG3C10_2:1a_E1 (blue).

Figure A.4 shows the comparison of the ^{1}H NMR spectra of PG3C10_2:1b (^{1}H NMR (600 MHz, MeOD) 4.20 – 3.43 (m, 31H), 2.38 (dt, J = 13.1, 7.9 Hz, 2H), 1.65 (q, J = 7.2 Hz, 2H), 1.41 – 1.28 (m, 13H), 0.94 (t, J = 6.9 Hz, 3H)) and PG3C10_2:1b_E1 (^{1}H NMR (600 MHz, MeOD) 4.21 – 3.46 (m, 14H), 2.37 (dt, J = 13.1, 7.8 Hz, 2H), 1.65 (p, J = 7.4 Hz, 2H), 1.40 – 1.27 (m, 13H), 0.94 (t, J = 6.9 Hz, 3H)).

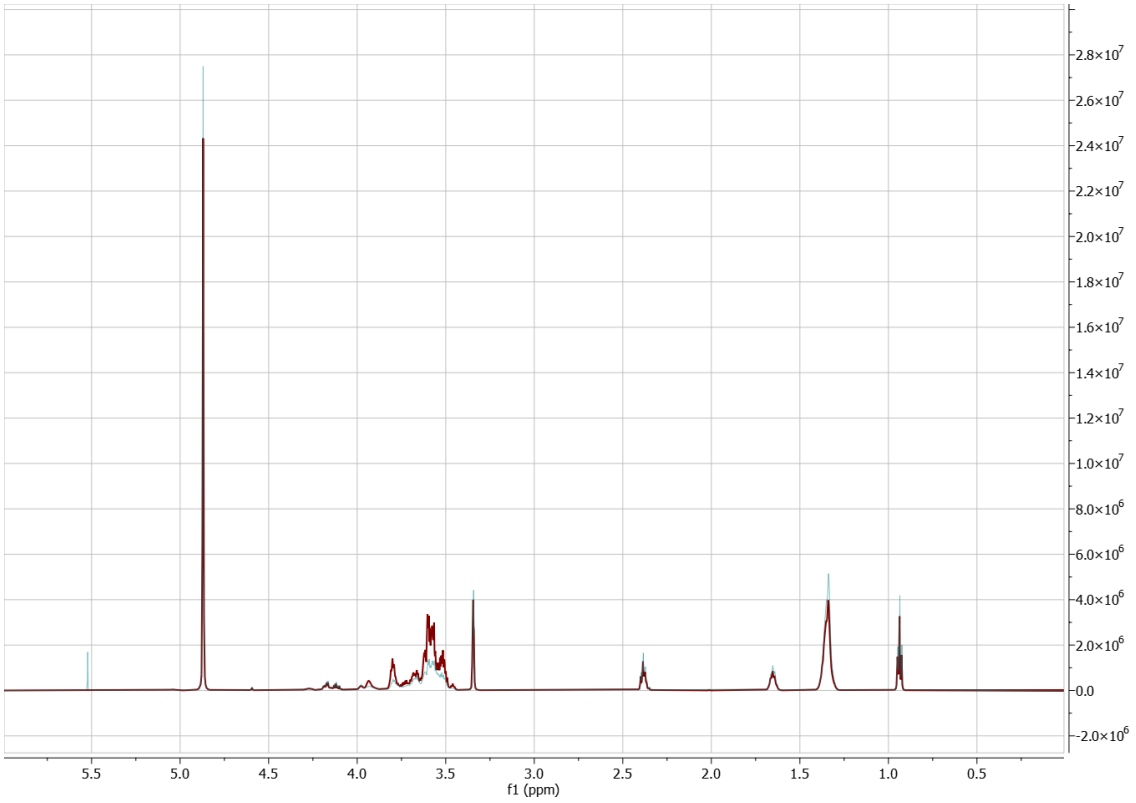

Figure A.4: Comparison of the ^{1}H NMR spectra of batch 2 before extraction (red) and after the first extraction (blue).

Figure A.5 shows the comparison of the ^{13}C NMR spectra of PG3C10_2:1b (^{13}C NMR (151 MHz, MeOD) 81.81, 80.03, 72.47, 72.21, 71.23, 71.15, 70.85, 70.82, 70.64, 69.66, 69.30, 68.18, 65.13, 62.92, 61.34, 61.15, 33.82, 33.55, 31.64, 29.18, 29.02, 28.81, 24.63, 22.33, 13.04) and PG3C10_2:1b_E1 (^{13}C NMR (151 MHz, MeOD) 174.06, 81.83, 80.06, 79.01, 72.52, 72.46, 72.21, 71.43, 71.13, 70.86, 70.83, 69.71, 69.29, 68.58, 68.18, 65.13, 62.94, 62.91, 61.35, 61.15, 60.40, 33.81, 33.55, 31.65, 29.18, 29.02, 28.81, 24.63, 22.33, 13.04).

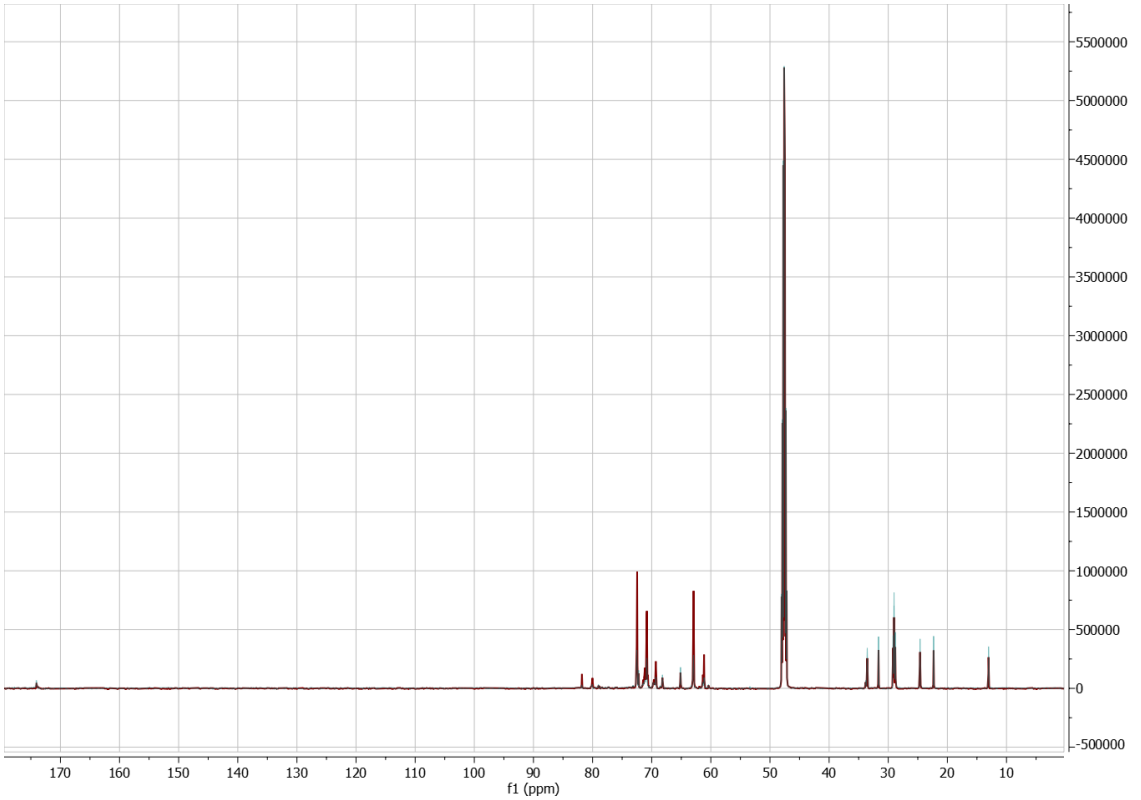

Figure A.5: Comparison of the ^{13}C NMR spectra of PG3C10_2:1b (red) and PG3C10_2:1b_E1 (blue).

Figure A.6 shows the comparison of the ^{1}H NMR spectra of PG3C10_10:1 (^{1}H NMR (600 MHz, MeOD) 4.20 – 3.41 (m, 160H), 2.44 – 2.31 (m, 2H), 1.65 (p, J = 7.7 Hz, 2H), 1.41 – 1.27 (m, 12H), 0.93 (t, J = 6.9 Hz, 3H)) and PG3C10_10:1_E1 (^{1}H NMR (600 MHz, MeOD) 4.59 (s, 1H), 4.30 – 3.42 (m, 19H), 2.41 – 2.33 (m, 2H), 1.65 (p, J = 7.3 Hz, 2H), 1.40 – 1.28 (m, 12H), 0.93 (t, J = 6.9 Hz, 3H)).

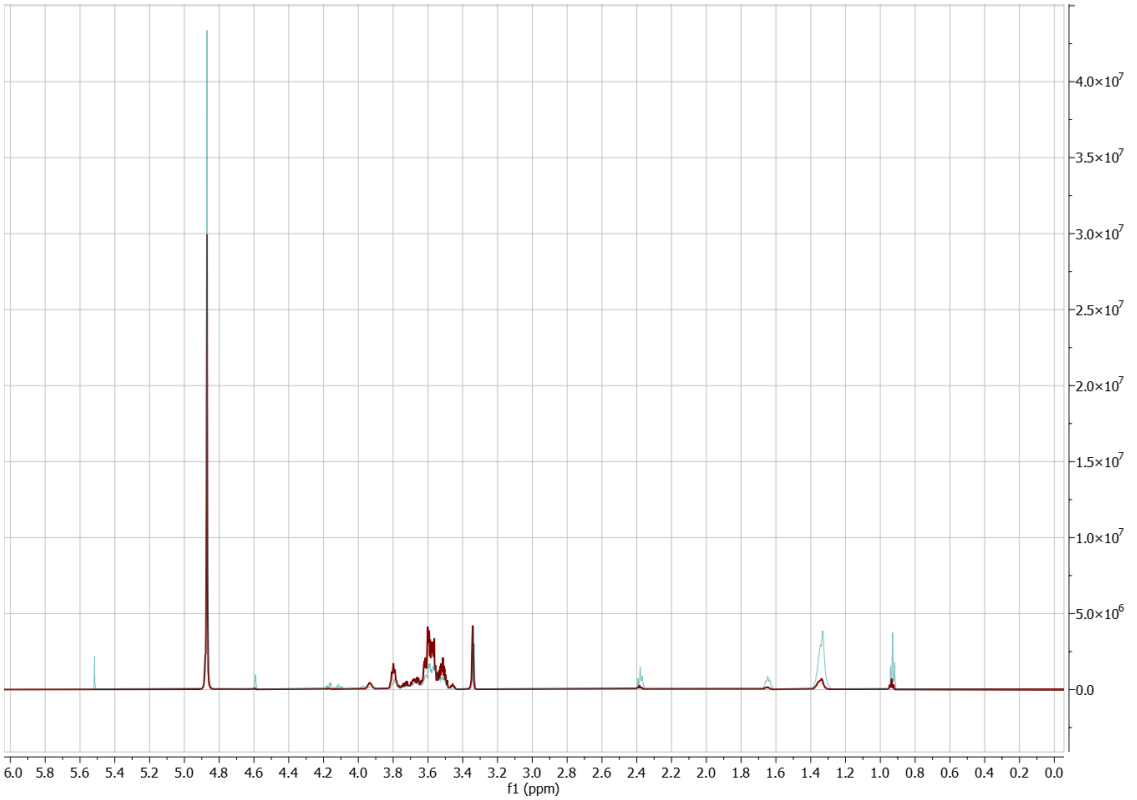

Figure A.6: Comparison of the ^{1}H NMR spectra of PG3C10_10:1 (red) and PG3C10_10:1_E1 (blue).

Figure A.7 shows the ^{13}C NMR spectrum of PG3C10_10:1 (^{13}C NMR (151 MHz, MeOD) 81.81, 80.02, 79.96, 72.49, 72.45, 72.21, 71.45, 71.27, 71.23, 71.15, 71.04, 70.85, 70.82, 70.64, 69.65, 69.34, 69.31, 69.27, 68.18, 65.13, 63.00, 62.92, 62.83, 61.34, 61.14, 33.55, 31.64, 29.17, 29.01, 28.80, 24.62, 22.32, 13.03) and PG3C10_10:1_E1 (^{13}C NMR (151 MHz, MeOD) 174.06, 81.82, 80.03, 78.88, 72.49, 72.21, 71.15, 70.85, 70.82, 69.66, 69.30, 68.19, 65.13, 62.92, 61.34, 61.14, 60.39, 33.79, 33.59, 33.54, 31.63, 29.17, 29.01, 28.80, 24.62, 22.32, 13.03).

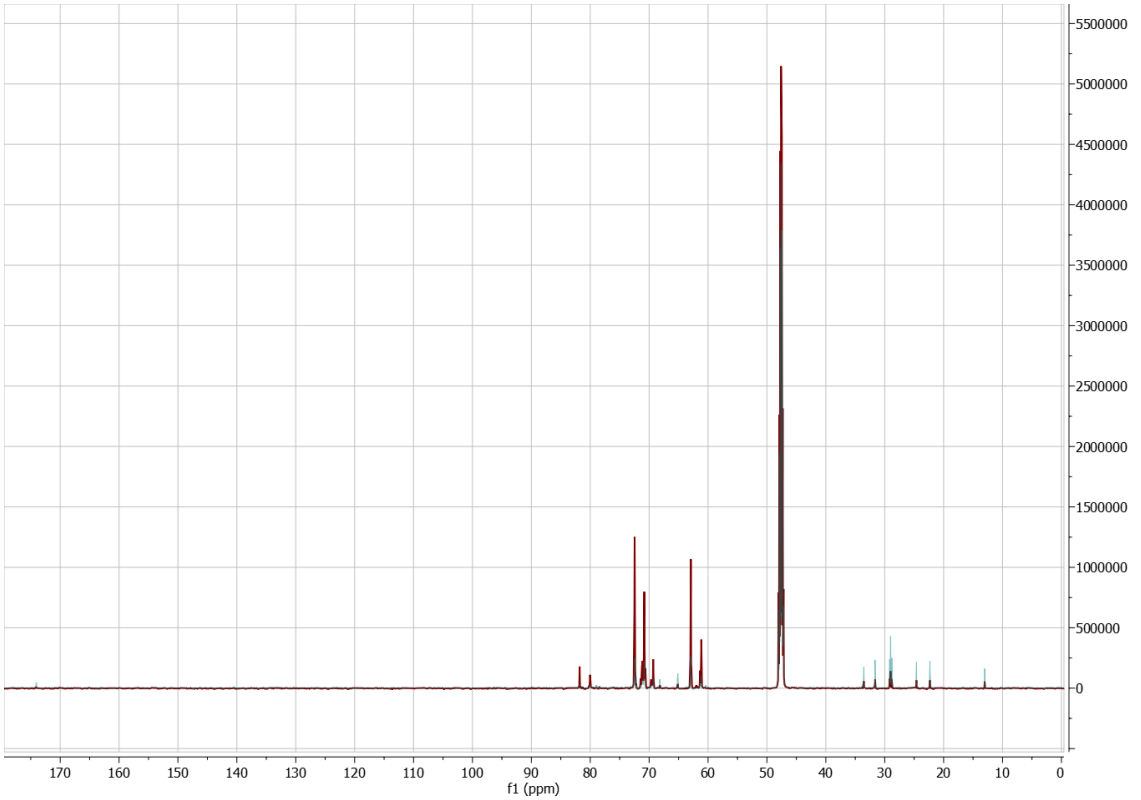

Figure A.7: Comparison of the ^{13}C NMR spectra of PG3C10_10:1 (red) and PG3C10_10:1_E1 (blue).

A.5 Surface tension curve for polyglycerol-3

Figure A.8 shows the graph of surface tension versus concentration for polyglycerol-3 when pendant drop tensiometry was performed using the concentration series in Table A.2.

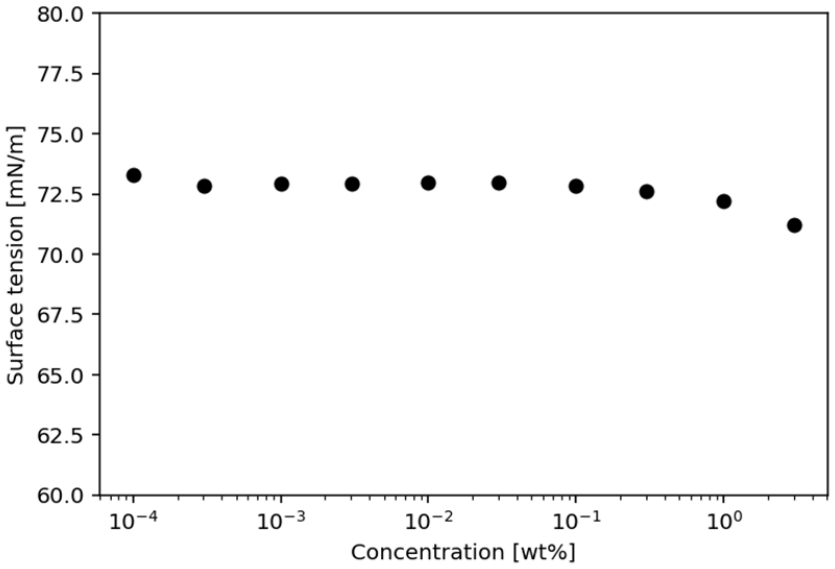

Figure A.8: Graph of surface tension versus concentration for polyglycerol-3.

A.6 IR spectra for PGEs synthesized through the solvent route

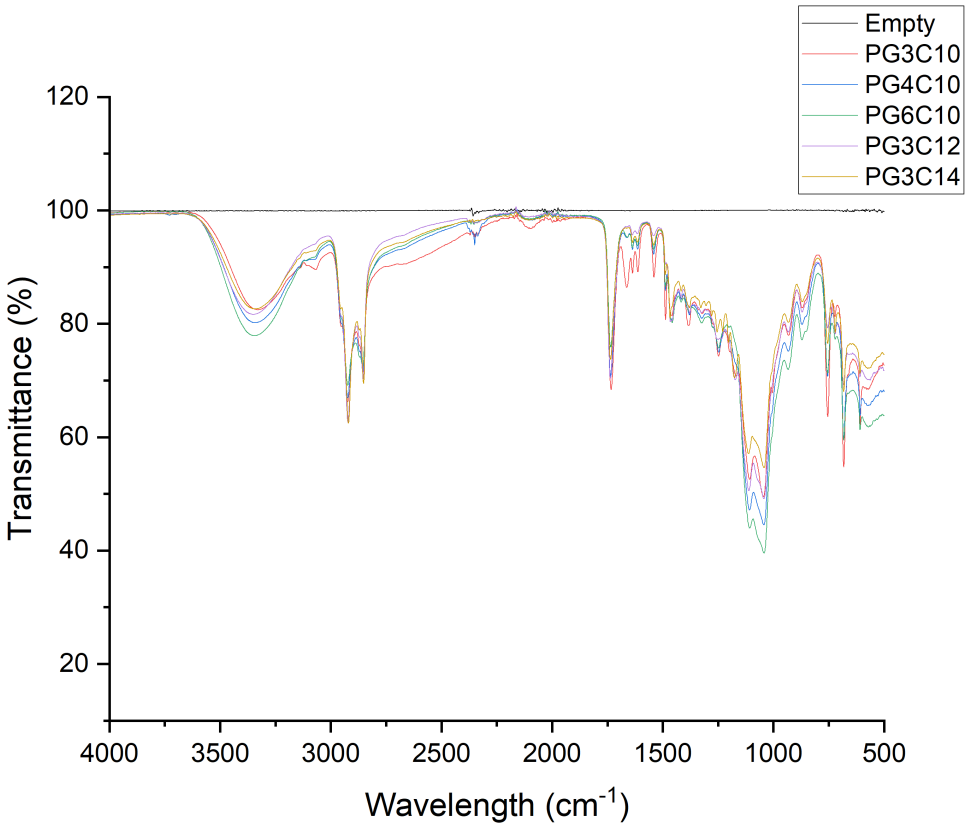

Figure A.9: IR spectra for PGEs synthesized through the solvent route, with the peak of the carbonyl functional group located at 1735 - 1740 cm^{-1}.

A.7 NMR data and spectra for PGEs synthesized through the solvent route

Figure A.10 is the ^{1}H NMR spectrum of PG3C10 (^{1}H NMR (600 MHz, MeOD) 8.83 (dt, J = 5.0, 1.6 Hz, 2H), 8.62 (tt, J = 7.9, 1.5 Hz, 1H), 8.11 – 8.04 (m, 2H), 4.29 – 3.33 (m, 15H), 2.32 – 2.25 (m, 2H), 1.61 – 1.50 (m, 2H), 1.33 – 1.17 (m, 13H), 0.84 (t, J = 6.9 Hz, 3H)). Figure A.11 is the ^{13}C NMR spectrum of PG3C10 (^{13}C NMR (151 MHz, MeOD) 174.04, 146.86, 141.67, 127.38, 81.81, 73.16, 72.47, 72.21, 71.15, 70.86, 70.83, 69.60, 69.28, 68.18, 65.13, 62.93, 61.34, 61.15, 60.40, 35.56, 33.80, 33.55, 31.64, 29.18, 29.02, 28.81, 24.63, 22.33, 13.04).

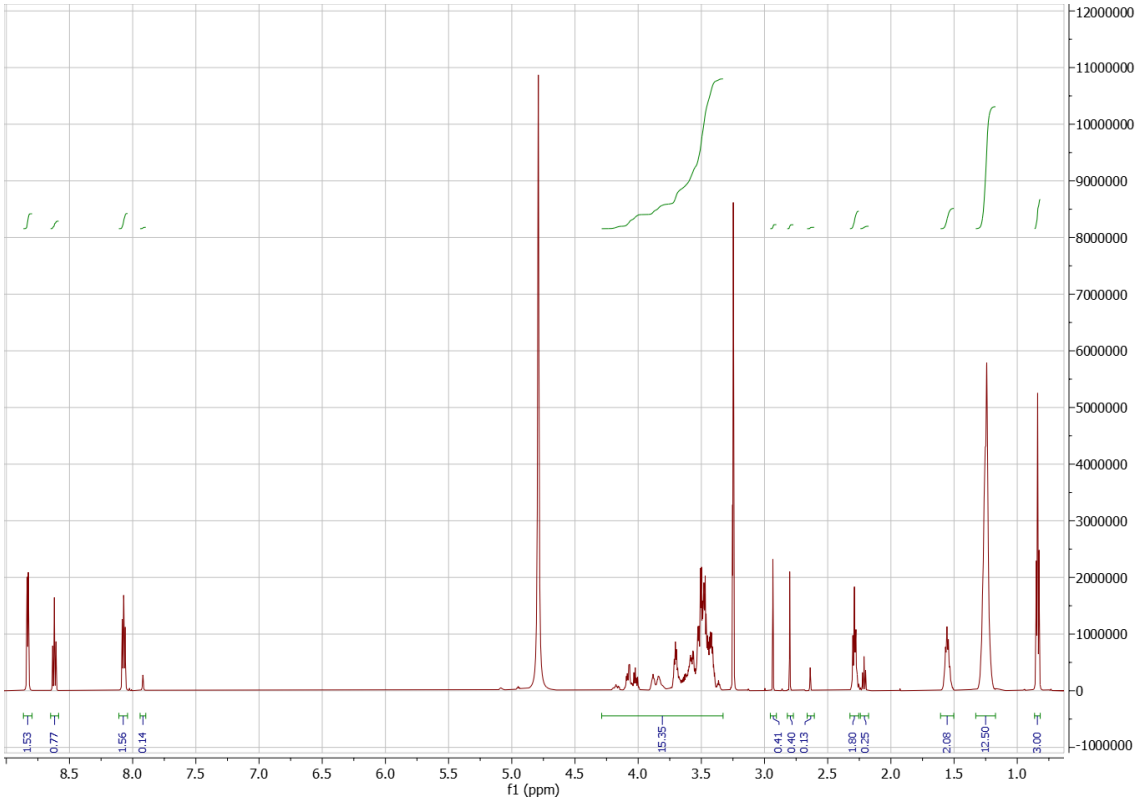

Figure A.10: ^{1}H NMR spectrum of PG3C10.

Figure A.12 is the ^{1}H NMR spectrum of PG4C10 (^{1}H NMR (600 MHz, MeOD) 8.91 – 8.78 (m, 1H), 8.61 (tt, J = 7.8, 1.6 Hz, 1H), 8.14 – 7.86 (m, 1H), 4.31 – 3.31 (m, 22H), 2.29 (td, J = 7.4, 4.5 Hz, 2H), 1.56 (h, J = 7.1 Hz, 2H), 1.33 – 1.19 (m, 12H), 0.84 (t, J = 6.9 Hz, 3H)). Figure A.13 is the ^{13}C NMR spectrum of PG4C10 (^{13}C NMR (151 MHz, MeOD) 174.05, 146.66, 141.83, 127.31, 81.82, 80.03, 72.49, 72.21, 71.45, 71.17, 71.04, 70.86, 70.83, 69.64, 69.29, 68.18, 65.14, 62.94, 61.34, 61.16, 33.81, 33.61, 33.55, 31.64, 29.18, 29.02, 28.81, 24.64, 22.33, 13.04).

Figure A.14 is the ^{1}H NMR spectrum of PG6C10 (1H NMR (600 MHz, MeOD) 8.86 – 8.80 (m, 1H), 8.61 (tt, J = 7.9, 1.5 Hz, 1H), 8.10 – 8.00 (m, 1H), 4.28 – 3.30 (m, 33H), 2.35 – 2.25 (m, 2H), 1.56 (q, J = 7.2 Hz, 2H), 1.34 – 1.18 (m, 12H), 0.85

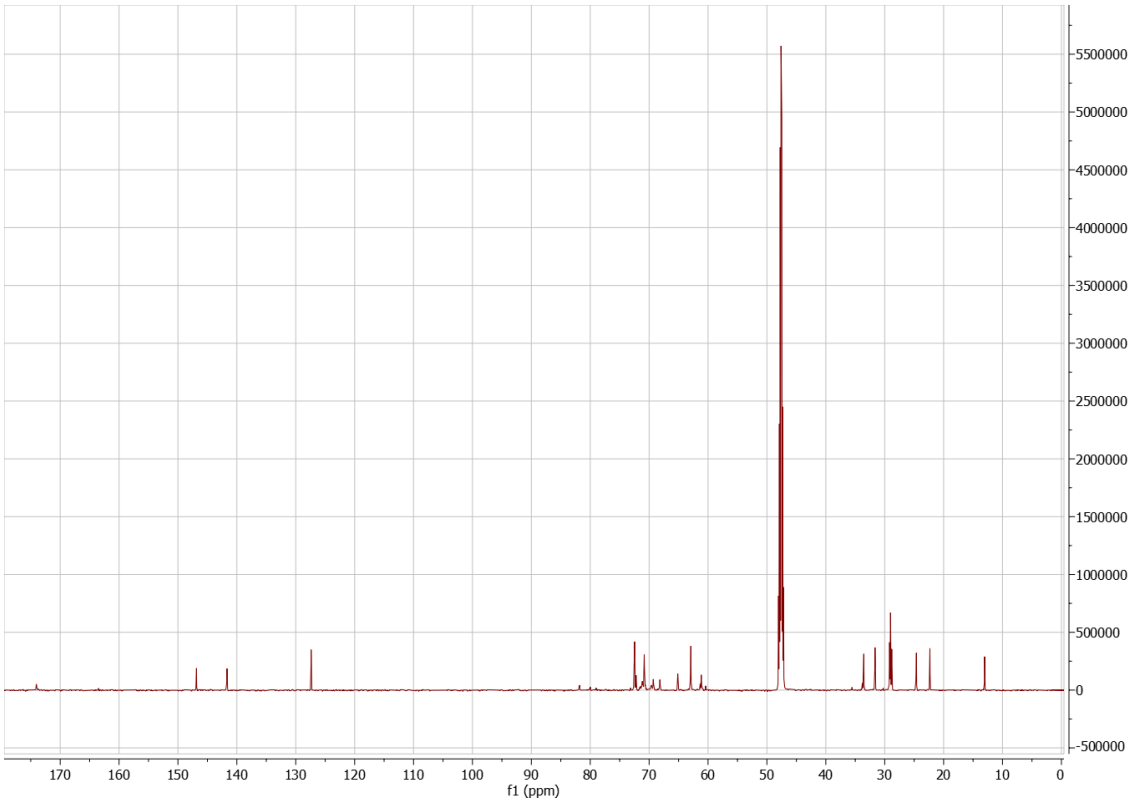

Figure A.11: ^{13}C NMR spectrum of PG3C10.

(t, J = 6.9 Hz, 3H)). Figure A.15 is the ^{13}C NMR spectrum of PG6C10 (^{13}C NMR (151 MHz, MeOD) 146.64, 141.85, 127.31, 81.82, 80.03, 74.07, 72.49, 72.22, 71.41, 71.17, 71.05, 70.87, 70.83, 69.62, 69.32, 69.26, 68.18, 65.14, 62.94, 61.35, 61.16, 33.81, 33.56, 31.65, 29.19, 29.02, 28.81, 24.64, 22.33, 13.05).

Figure A.16 is the ^{1}H NMR spectrum of PG3C12 (^{1}H NMR (600 MHz, MeOD) 4.28 – 3.31 (m, 16H), 2.36 – 2.25 (m, 2H), 1.56 (h, J = 7.0 Hz, 2H), 1.41 – 1.09 (m, 17H), 0.85 (t, J = 6.9 Hz, 3H)). Figure A.17 is the ^{13}C NMR spectrum of PG3C12 (^{13}C NMR (151 MHz, MeOD) 174.06, 146.14, 142.19, 127.14, 81.80, 80.02, 73.16, 72.47, 72.21, 71.16, 70.86, 70.82, 69.63, 69.29, 68.18, 65.13, 62.92, 61.34, 61.15, 60.40, 33.79, 33.55, 31.68, 29.34, 29.21, 29.07, 29.02, 28.81, 24.63, 22.34, 13.04).

Figure A.18 is the ^{1}H NMR spectrum of PG3C14 (^{1}H NMR (600 MHz, MeOD) 8.82 (dt, J = 5.1, 1.6 Hz, 1H), 8.11 – 8.00 (m, 1H), 4.38 – 3.32 (m, 16H), 2.34 – 2.25 (m, 2H), 1.56 (h, J = 6.8 Hz, 2H), 1.25 (d, J = 17.1 Hz, 21H), 0.85 (t, J = 7.0 Hz, 3H)). Figure A.19 is the ^{13}C NMR spectrum of PG3C14 (^{13}C NMR (151 MHz, MeOD) 146.54, 141.90, 127.28, 72.47, 72.21, 71.16, 70.86, 70.83, 69.65, 69.29, 68.19, 65.14, 62.93, 61.33, 61.15, 42.56, 33.81, 33.56, 31.68, 29.37, 29.22, 29.08, 29.02, 28.82, 24.64, 22.34, 13.05).

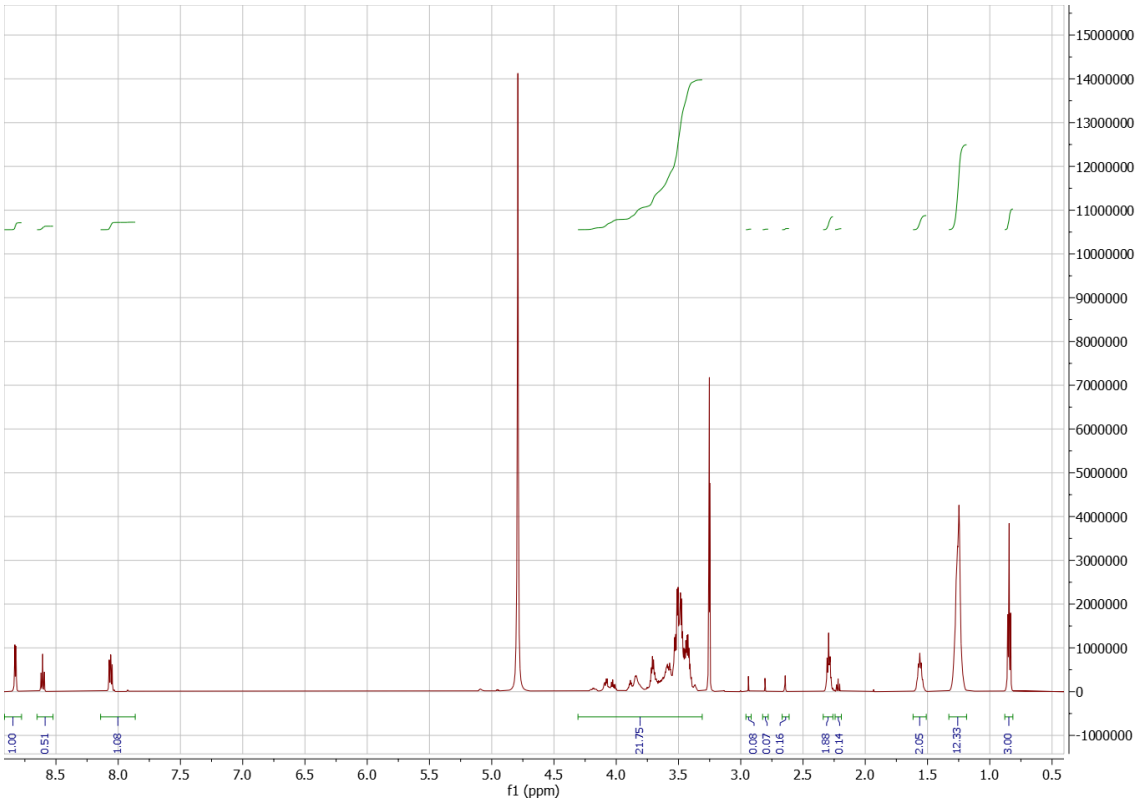

Figure A.12: ^{1}H NMR spectrum of PG4C10.

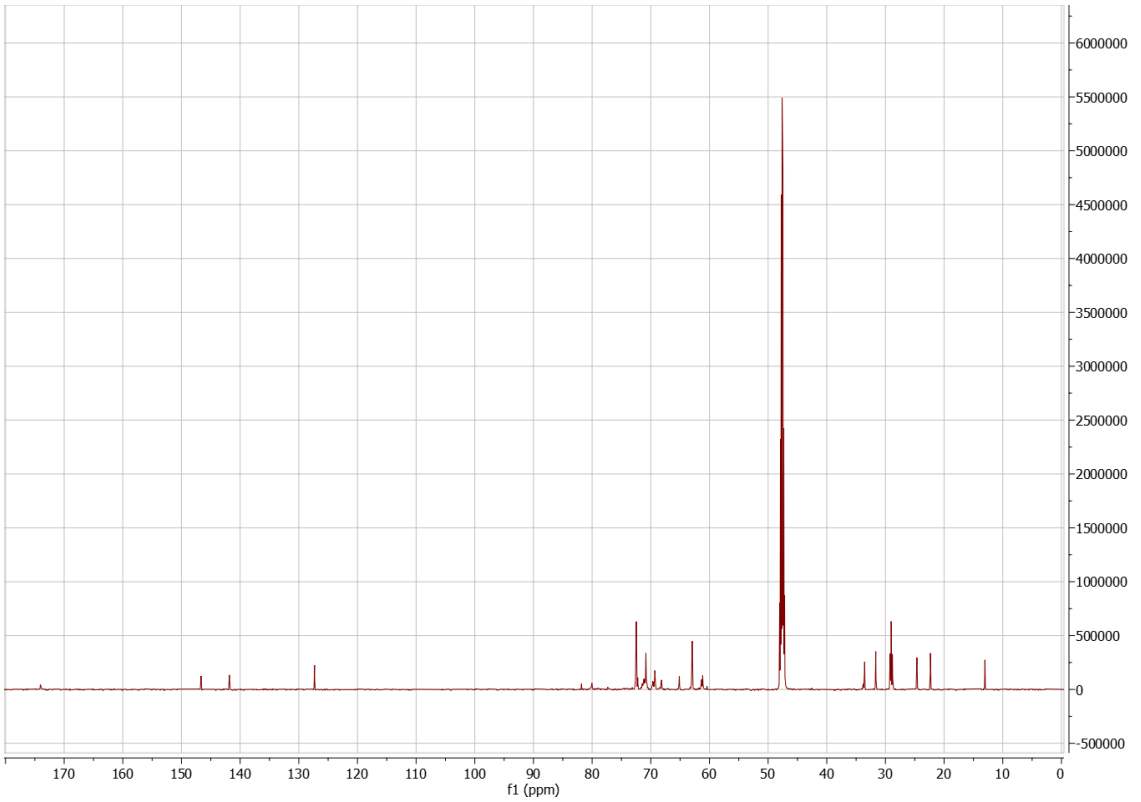

Figure A.13: ^{13}C NMR spectrum of PG4C10.

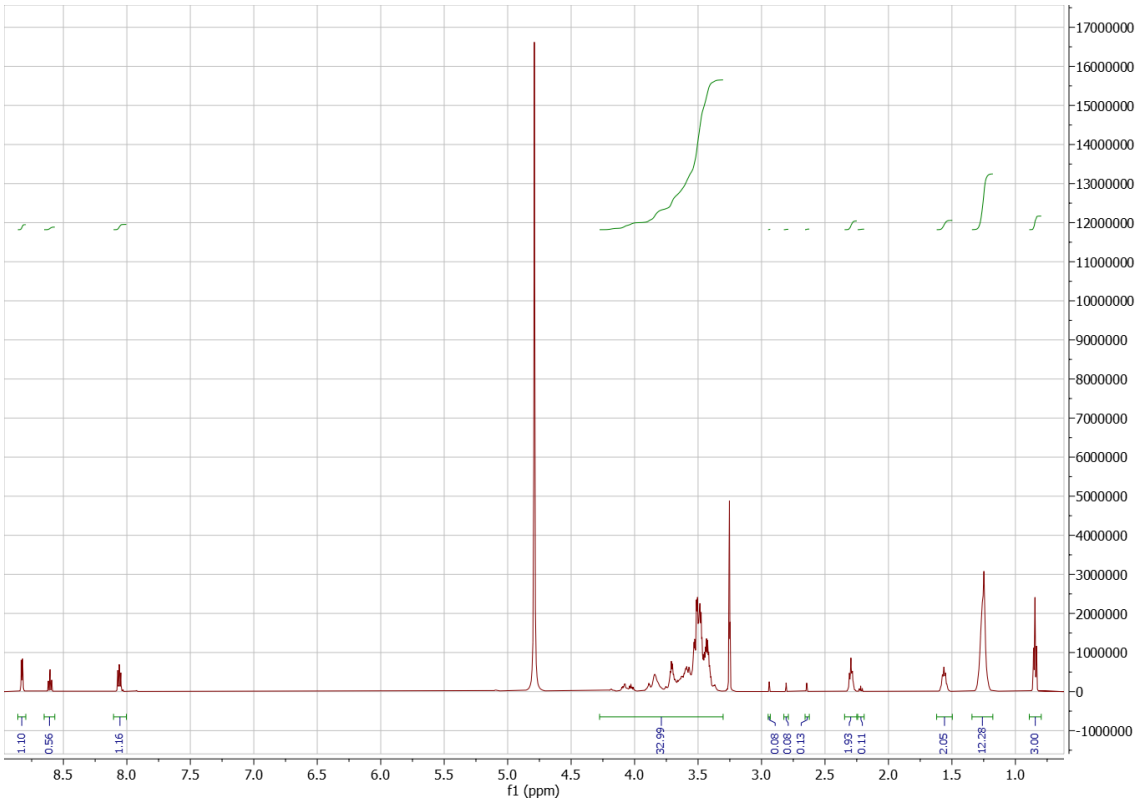

Figure A.14: ^{1}H NMR spectrum of PG6C10.

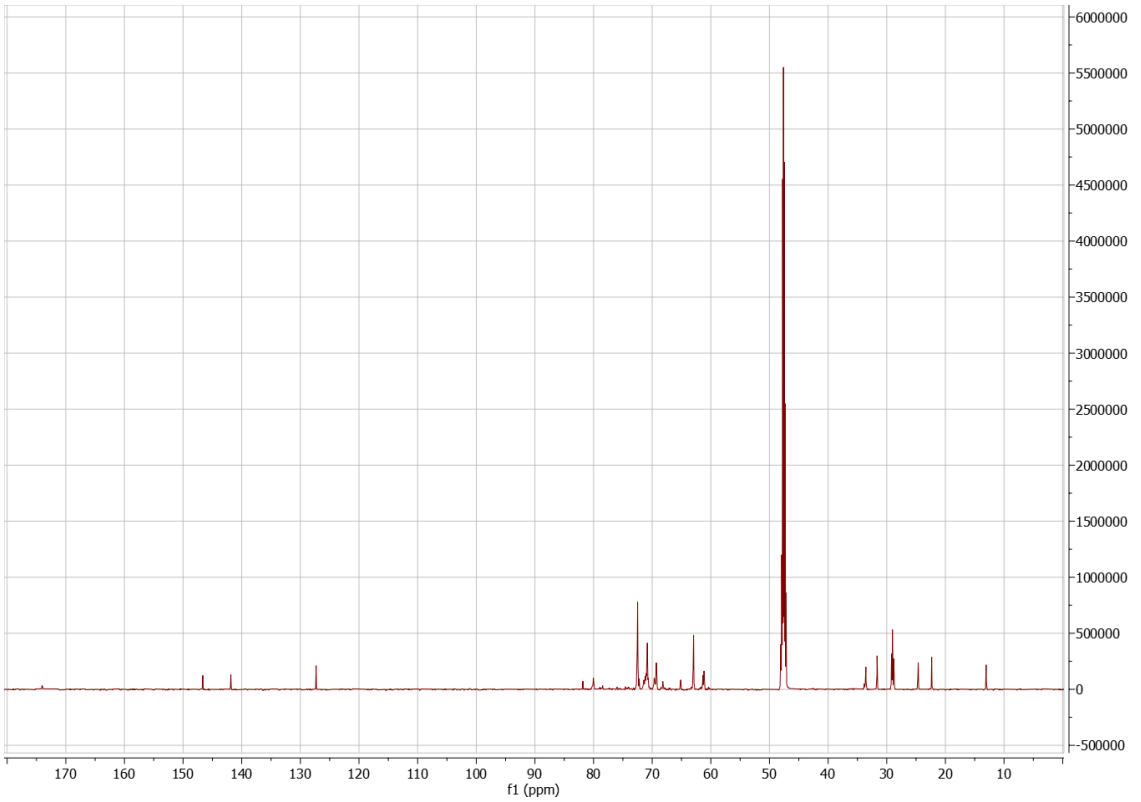

Figure A.15: ^{13}C NMR spectrum of PG6C10.

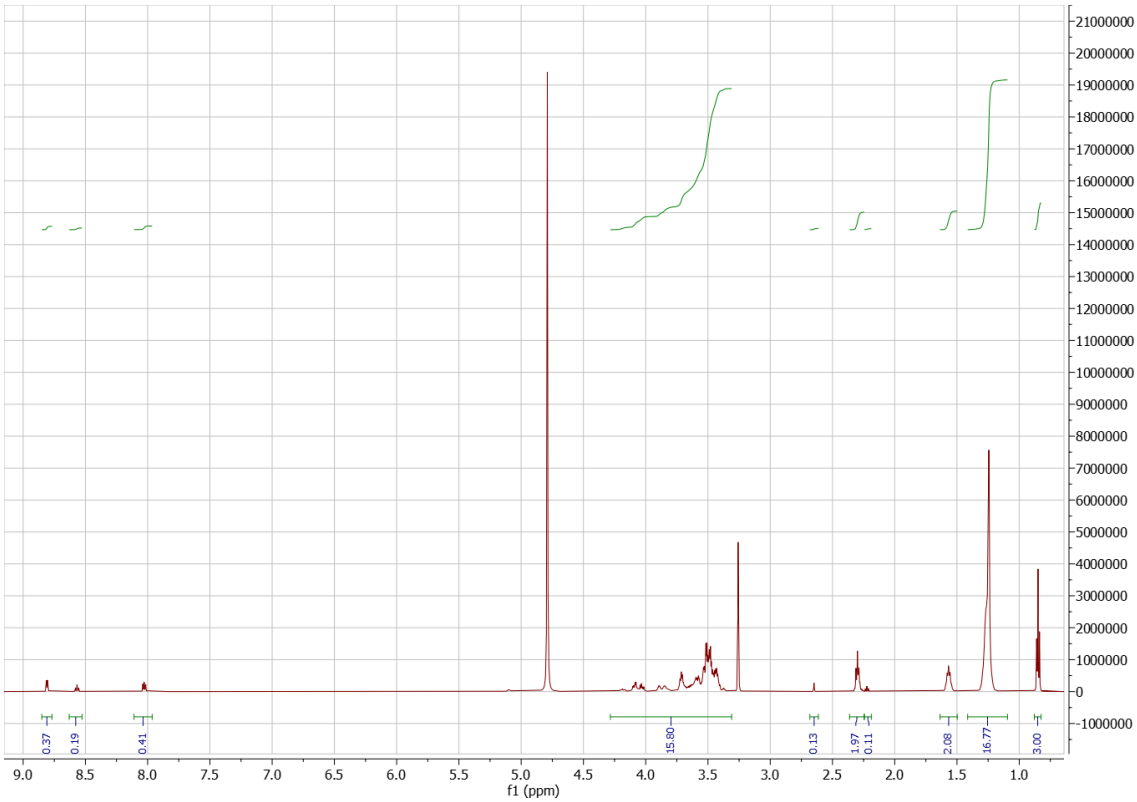

Figure A.16: ^{1}H NMR spectrum of PG3C12.

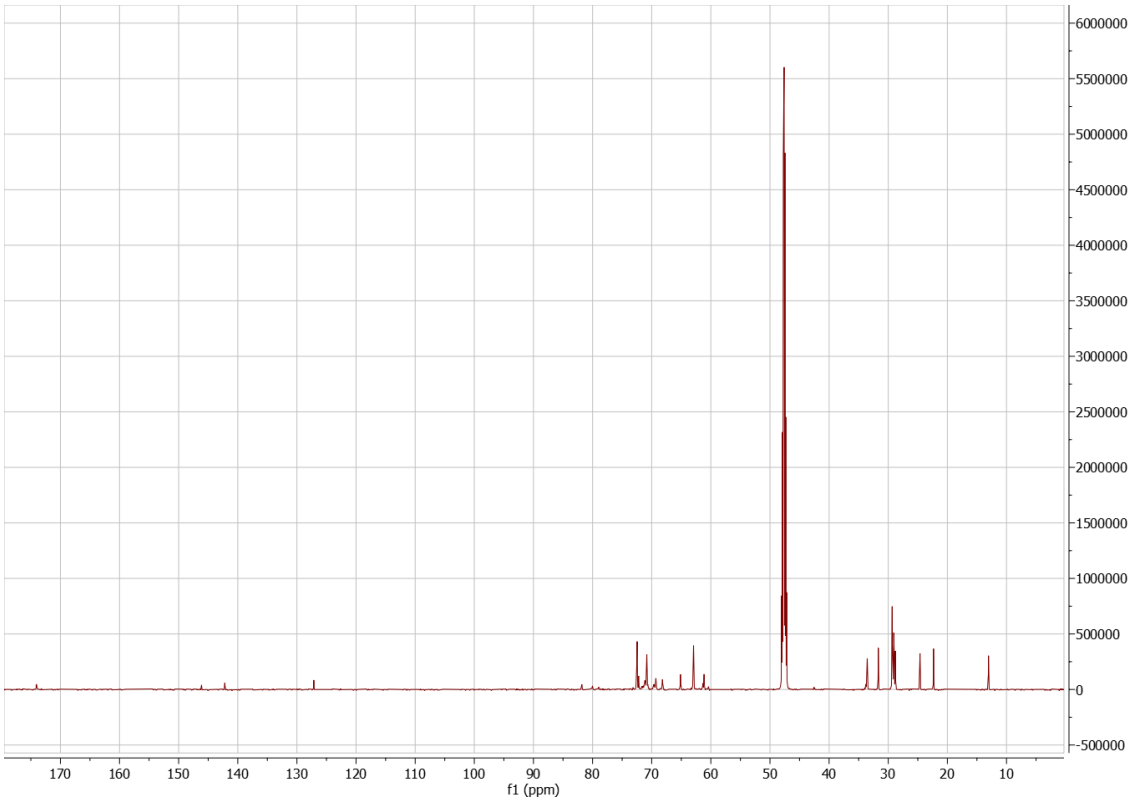

Figure A.17: ^{13}C NMR spectrum of PG3C12.

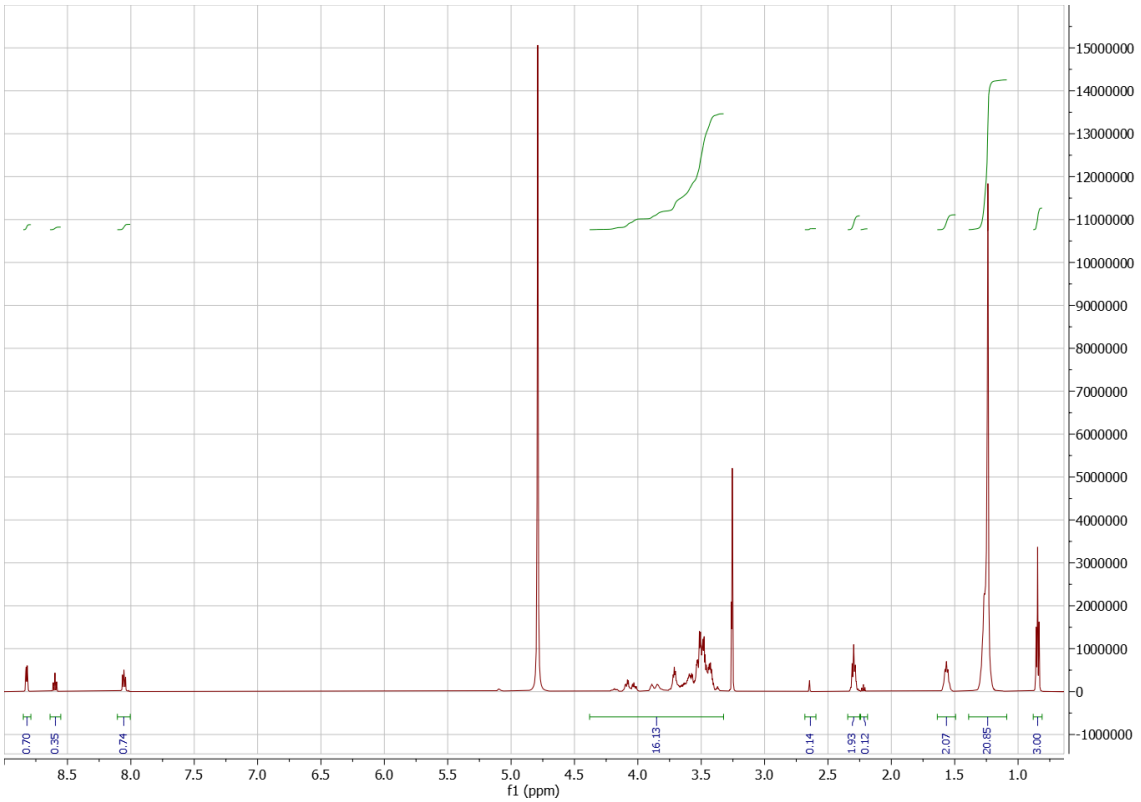

Figure A.18: ^{1}H NMR spectrum of PG3C14.

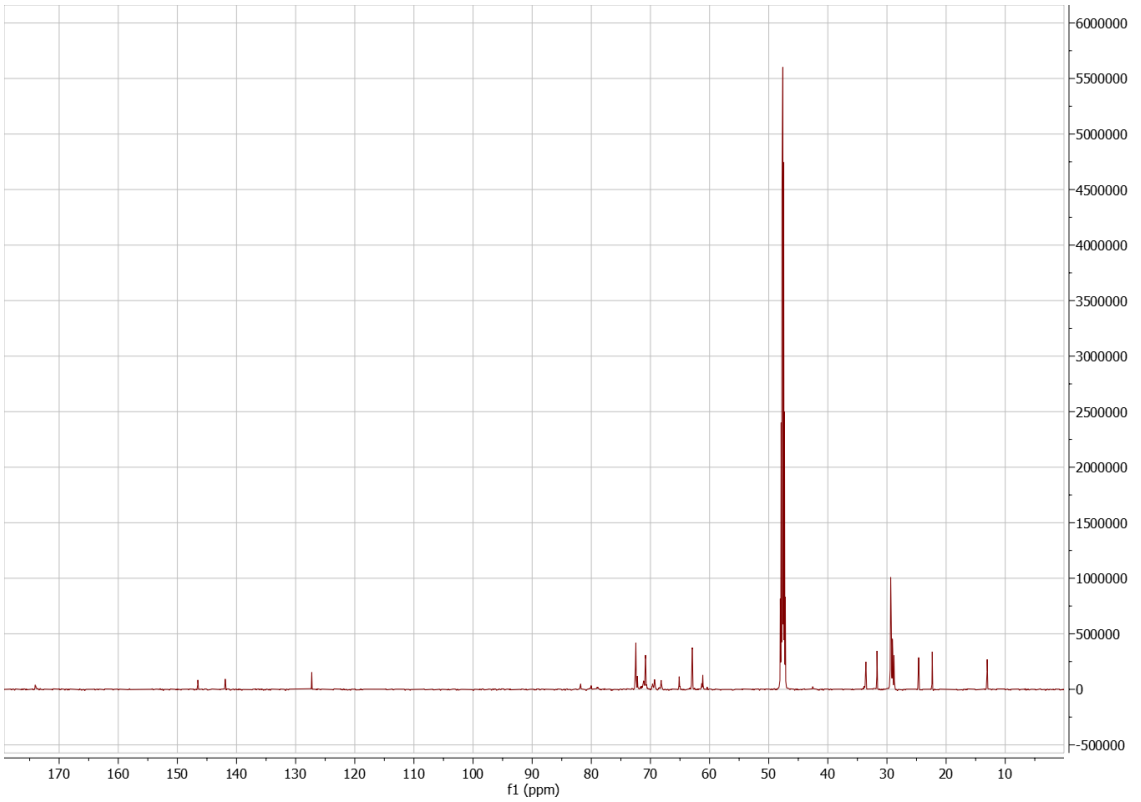

Figure A.19: ^{13}C NMR spectrum of PG3C14.

DEPARTMENT OF CHEMISTRY AND CHEMICAL ENGINEERING
CHALMERS UNIVERSITY OF TECHNOLOGY
Gothenburg, Sweden
www.chalmers.se

CHALMERS
UNIVERSITY OF TECHNOLOGY